11-3-2020

Airway microbiota-host interactions regulate secretory leukocyte protease inhibitor levels and influence allergic airway inflammation

Natalia Jaeger
Washington University School of Medicine in St. Louis

Ryan T McDonough
Washington University School of Medicine in St. Louis

Anne L Rosen
Washington University School of Medicine in St. Louis

Ariel Hernandez-Leyva
Washington University School of Medicine in St. Louis

Naomi G Wilson
Washington University School of Medicine in St. Louis

See next page for additional authors

Cell Reports

Article

Airway Microbiota-Host Interactions Regulate Secretory Leukocyte Protease Inhibitor Levels and Influence Allergic Airway Inflammation

Graphical Abstract

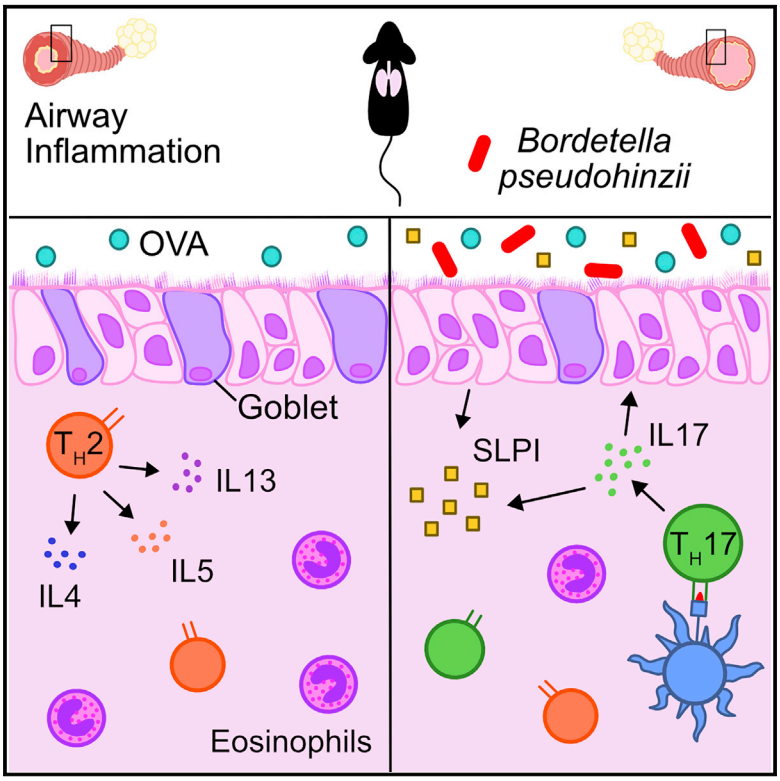

Authors

Natalia Jaeger, Ryan T. McDonough, Anne L. Rosen, ..., Leonard B. Bacharier, Chyi-Song Hsieh, Andrew L. Kau

Correspondence

akau@wustl.edu

In Brief

Asthma is known to be modified by airway microbes. Jaeger et al. use a murine-adapted bacterium to show that airway colonization evokes a Th17 response associated with increased SLPI, an antimicrobial peptide, and protection from lung inflammation. In people, SLPI was correlated with airway microbiota composition.

Highlights

- *Bordetella pseudohinzii* (*Bph*) colonizes the mouse airway and induces a Th17 response
- *Bph*-colonized mice show reduced allergic airway inflammation (AAI) in an asthma model
- The antimicrobial peptide SLPI is linked to diminished AAI and is regulated by IL-17A
- In humans, upper airway microbiota composition was correlated with SLPI abundance

Jaeger et al., 2020, Cell Reports *33*, 108331
November 3, 2020
https://doi.org/10.1016/j.celrep.2020.108331

CellPress

Cell Reports

CellPress
OPEN ACCESS

Article

Airway Microbiota-Host Interactions Regulate Secretory Leukocyte Protease Inhibitor Levels and Influence Allergic Airway Inflammation

Natalia Jaeger,[1] Ryan T. McDonough,[1] Anne L. Rosen,[1] Ariel Hernandez-Leyva,[1] Naomi G. Wilson,[1] Michael A. Lint,[1] Emilie V. Russler-Germain,[2] Jiani N. Chai,[2] Leonard B. Bacharier,[3,4] Chyi-Song Hsieh,[2] and Andrew L. Kau[1,5,*]

[1]Division of Allergy and Immunology, Department of Medicine and Center for Women's Infectious Disease Research, Washington University School of Medicine, St. Louis, MO 63110, USA

[2]Division of Rheumatology, Department of Medicine, Washington University School of Medicine, St. Louis, MO 63110, USA

[3]Division of Allergy, Immunology and Pulmonary Medicine, Department of Pediatrics, Washington University School of Medicine, St. Louis, MO 63110, USA

[4]Present address: Division of Allergy, Immunology and Pulmonary Medicine, Department of Pediatrics, Monroe Carell Jr Children's Hospital at Vanderbilt University Medical Center, Nashville, TN 37232, USA

[5]Lead Contact

*Correspondence: akau@wustl.edu

https://doi.org/10.1016/j.celrep.2020.108331

SUMMARY

Homeostatic mucosal immune responses are fine-tuned by naturally evolved interactions with native microbes, and integrating these relationships into experimental models can provide new insights into human diseases. Here, we leverage a murine-adapted airway microbe, *Bordetella pseudohinzii* (*Bph*), to investigate how chronic colonization impacts mucosal immunity and the development of allergic airway inflammation (AAI). Colonization with *Bph* induces the differentiation of interleukin-17A (IL-17A)-secreting T-helper cells that aid in controlling bacterial abundance. *Bph* colonization protects from AAI and is associated with increased production of secretory leukocyte protease inhibitor (SLPI), an antimicrobial peptide with anti-inflammatory properties. These findings are additionally supported by clinical data showing that higher levels of upper respiratory SLPI correlate both with greater asthma control and the presence of *Haemophilus,* a bacterial genus associated with AAI. We propose that SLPI could be used as a biomarker of beneficial host-commensal relationships in the airway.

INTRODUCTION

The airway microbiota is increasingly recognized for its diverse roles in respiratory inflammatory diseases, especially asthma. Microbiologic surveys of upper and lower airway samples have demonstrated that individuals with asthma harbor distinct microbial signatures associated with various facets of the disease. In early childhood, the presence of select bacteria within the upper airway, including *Haemophilus*, *Streptococcus*, and *Moraxella* (HSM) species, has been associated with later development of asthma (e.g., Bisgaard et al., 2007, 2010), although healthy individuals can also harbor these organisms, suggesting compensatory host responses that may mitigate asthma risk. In addition to predisposing human to asthma, the airway microbiota has been proposed as a factor that influences an individual's clinical phenotype, including the immunologic markers associated with disease and response to therapy, referred to as an asthma endotype. Although the most established asthma endotype is associated with allergic T-helper 2 (Th2) responses, characterized by the production of interleukin-4 (IL-4), IL-5, and IL-13 cytokines, T-helper 17 (Th17) responses, defined by the production of IL-17A, is also of particular interest. In clinical studies, higher degrees of IL-17A expression have been associated with severe asthma and correlate with increased numbers of airway neutrophils and resistance to corticosteroid treatments (Chesné et al., 2014; Östling et al., 2019). Animal models have additionally shown that the adoptive transfer of allergen-specific Th17 cells contributes to allergic airway inflammation (AAI) and drives airway neutrophilia (McKinley et al., 2008; Wakashin et al., 2008). In contrast, other studies suggest that IL-17A may directly antagonize Th2 responses and reduce AAI (Barlow et al., 2011; Choy et al., 2015; Newcomb et al., 2013; Schnyder-Candrian et al., 2006).

How airway microbes shape asthma endotypes and influence the particular clinical features of the disease is an area of active investigation. The importance of human airway microbes, such as *Haemophilus influenzae* (McCann et al., 2016), *Streptococcus pneumoniae* (Preston et al., 2007; Preston et al., 2011), and *Moraxella catarrhalis* (Alnahas et al., 2017), has been translated to animal models of asthma by demonstrating that respiratory exposure to these microbes directly affects AAI. Although these studies have confirmed the potential of select airway bacteria to

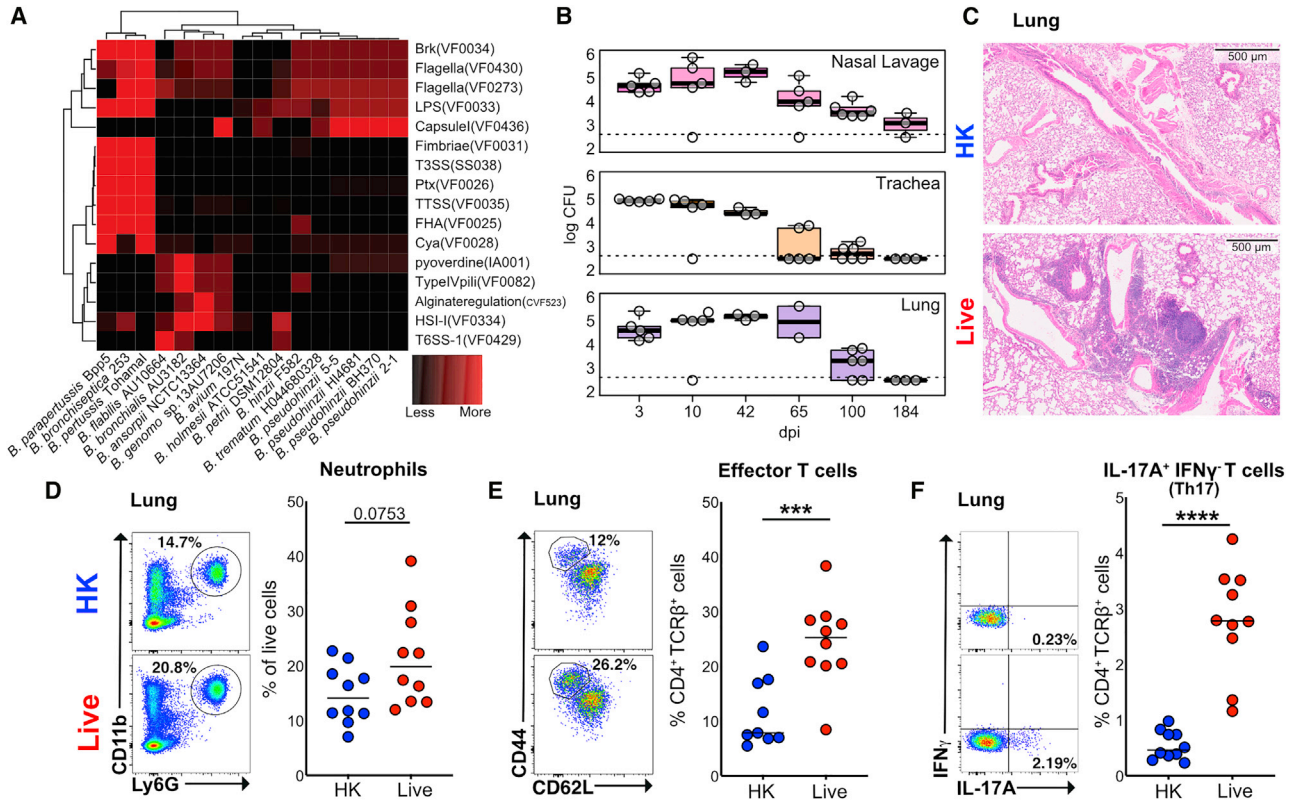

Figure 1. *Bordetella pseudohinzii* (*Bph*) Induces a Th17 Response in the Lungs of Colonized Mice

(A) Comparison of the abundance of virulence factor classes encoded in the genomes of members in the genus *Bordetella*. Virulence factors were identified by sequence alignment to the Virulence Factor Database (VFDB) and binned into functional groups defined by VFDB (Chen et al., 2016). Assemblies of *Bph* isolates described in this study (2-1 and 5-5) are also shown.

(B) Recovery of *Bph* from respiratory tract samples over a 184-day period. CFUs per section of tissue or mL of lavage fluid are shown. Box indicates 25th and 75th percentiles and whiskers are 1.5 × interquartile range. n = 2–6 mice per time point.

(C) Representative hematoxylin and eosin staining of mice that received either HK (top panel) or live (bottom panel) *Bph* taken 60 days after inoculation.

(D–F) Flow cytometry of lung tissue digests from mice 30 days after that received HK (blue) or live *Bph* (red) inoculation. n = 9–10 mice/group, combined from two independent experiments.

(D) Neutrophils as a percentage of live cells from lung. Neutrophils were defined as $CD11b^{+}Ly6G^{+}$.

(E) Percentage of Teff ($CD4^{+}TCR\beta^{+}FoxP3^{-}CD44^{hi}CD62L^{lo}$) cells from the lungs as a percentage of total T-helper cells.

(F) Percentages of IL-$17A^{+}IFN\gamma^{-}$-secreting T-helper 17 (Th17) cells from the lungs.

Statistical significance: Mann-Whitney U test. Horizontal lines indicate median values. *$p < 0.05$; **$p < 0.01$; ***$p < 0.001$; ****$p < 0.0001$.

modulate AAI, one important limitation of this approach is that mouse models using bacteria from the human airway may not establish a host-microbe interaction that adequately recapitulates important interactions observed in humans. This is especially relevant for asthma because many of the microbes implicated in worsening AAI from clinical studies only transiently colonize mice (Unhanand et al., 1992). These constraints on colonization limit our ability to use mice to model the effects of microbes that would be expected to persist in human airways. One possible solution to the challenge of modeling the effects of microbial exposure in murine models is to use natural members of the mouse microbiota. Experiments incorporating "wild" mouse microbes in a laboratory setting have been used to better align mouse models of endotoxemia (Rosshart et al., 2019), viral infections (Beura et al., 2016), and tumorigenesis (Rosshart et al., 2017) to human disease.

Here, we describe the host response to *Bordetella pseudohinzii* (*Bph*), a recently described murine respiratory microbe (Clark et al., 2016; Ivanov et al., 2016) that is also found in wild rodents (Loong et al., 2018), and its effects on a model of AAI. Although *Bph* persists in the respiratory tract of mice for months after inoculation (Dewan et al., 2019), the preponderance of infections do not lead to overt signs of illness (Hayashimoto et al., 2012). Others have reported that despite its apparent benign effects on mice, *Bph* can induce changes in pulmonary immune parameters (e.g., neutrophilia), leading to concerns about *Bph* possibly confounding murine pulmonary disease models (Clark et al., 2016, 2017; Perniss et al., 2018). On the other hand, we speculated that studying a bacterium within the context of AAI that evolved to reside in the murine respiratory tract and was not transplanted from humans may provide unique insights into how prolonged exposure to a respiratory microbe affects

pulmonary inflammation. We found that *Bph* induces a marked Th17 response in mice that is associated with protection from AAI and stimulates the production of the antimicrobial protein secretory leukocyte protease inhibitor (SLPI). These findings are further supported by clinical data showing that increased nasal SLPI is correlated with greater asthma control and differences in bacterial composition within the upper airway microbiota.

RESULTS

Bph Colonizes the Mouse Respiratory Tract

We first wanted to contrast *Bph* to the "classical" bordetellae strains (*Bordetella pertussis*, *Bordetella parapertussis*, and *Bordetella bronchiseptica*) that are well-known causes of respiratory infections to better understand its virulence potential. To accomplish this, we compared known *Bordetella* reference strains and our own *Bph* isolate assemblies (designated 2-1 and 5-5) to a database of known bacterial virulence factors (Chen et al., 2016; Figure 1A). This analysis confirmed that *Bph* lacked the virulence factors associated with classical pathogenic *Bordetella* strains, including the genes for Pertussis toxin (Ptx), Filamentous Hemagglutinin (FHA), and the type III secretion system (T3SS).

To directly assess the *in vivo* impact of *Bph* colonization on mice, we intranasally inoculated C57BL/6 6- to 8-week-old mice with $\sim 10^4$ colony-forming units (CFUs) of bacteria and collected tissues from groups of mice over a 6-month period. *Bph* was consistently recovered from the nasal lavage, trachea, and lung for 3 months after initial colonization (Figure 1B). Despite this persistent colonization, we did not observe significant weight loss in *Bph*-colonized mice compared to control mice over a 3-month period (Figure S1A), nor observe sneezing (Clark et al., 2016; Hayashimoto et al., 2012), tachypnea, poor grooming, or decreased activity. Consistent with earlier descriptions of *Bph* mouse colonization and the lack of virulence factors found in classical bordetellae, these results indicated that *Bph* colonization was persistent and associated with a mild phenotype (Clark et al., 2016; Dewan et al., 2019; Ivanov et al., 2016; Perniss et al., 2018).

Colonization with *Bph* Induces Th17 Cells in the Lung

To better understand the effects of *Bph* on the host, we performed microscopic examination of the lungs of wild-type (WT) mice, which demonstrated the formation of lymphoid aggregates, consistent with inducible bronchus associated lymphoid tissue (iBALT; Marin et al., 2019), that was first detectable 10 days post-colonization, present in all colonized mice by 28 days, and persistent out to 6 months after initial colonization (Figures 1C, S1B, and S1C). These results imply that *Bph* elicits an adaptive immune response that we further investigated by performing immunophenotyping on lung immune cell populations. After 28 days of colonization (Figure S1D), we observed a trend toward an increase in neutrophils in lung tissue, as previously observed (Clark et al., 2016), accompanied by a decrease in eosinophils in mice colonized with *Bph* compared to mice undergoing mock colonization with 10^4 CFU heat-killed (HK) bacteria (Figures 1D and S1E). This number of HK bacteria equals the number of bacteria used in the live inoculum and contains considerably (~10,000 fold) fewer HK bacteria than other models intended to elicit a pulmonary immune response (Amezcua Vesely et al., 2019; Chen et al., 2011). Among T cell subsets, effector T cells (Teff) and T regulatory (Treg) cells were increased in colonized mice compared to controls (Figures 1E and S1F). Additional characterization of $CD4^+$ T cells by intracellular staining for cytokines showed that there was a marked increase in the percentages of IL-17A-expressing ($TCR\beta^+CD4^+IL\text{-}17A^+IFN\gamma^-$, referred to here as Th17) but not interferon gamma ($IFN\gamma$)-expressing (Th1) T cells (Figures 1F, S1G, and S1L) in colonized mice compared to mock-colonized controls. Examination of the non-$CD4^+$ T cell immune compartment showed no differences in IL-$17A^+$ cells between mice that received live or HK *Bph* (Figure S1H), nor did we see an increase in transcripts for the constant regions of T cell receptor gamma ($TCR\gamma$) or $TCR\delta$ (Table S1). Although we cannot absolutely exclude another *in vivo* source of IL-17A by *ex vivo* restimulation and intracellular cytokine staining, our data are most consistent with an expansion of Th17, rather than $\gamma\delta$-T cells, in response to *Bph*. These changes in immune cell subtypes within the lung were also accompanied by increases in Teff, Th17, and Treg cells in the spleens of *Bph*-colonized mice, demonstrating that airway colonization was also associated with immune changes detectable at distant tissues (Figures S1I, S1J, and S1K).

Bph Airway Colonization Induces a Th17 Immune Response

We next performed RNA sequencing (RNA-seq) on whole lungs from colonized and control mice 7 weeks after inoculation to determine the effects of *Bph* colonization on transcriptional regulation. Analysis of transcriptomic data using gene set enrichment analysis (GSEA) confirmed *Bph* markedly upregulated functions involved in the immune response in persistently colonized animals (Figure 2A). The most markedly upregulated pathway in colonized mice was associated with the intestinal immune response for immunoglobulin A (IgA) production. Examination of leading-edge genes (i.e., genes driving the enrichment score) from this pathway showed that many of the most strongly enhanced transcripts are also associated with iBALT formation, including genes for mucosal immune activation (*Icos*, *Icosl*, *CD40*, and *CD40lg*) and antibody generation (*Aicda* and *Pigr*; Figure 2B, top panel; Table S1). Genes involved in T cell differentiation pathways, including Th17 cell signaling and differentiation, were also enriched in colonized mice compared to controls, including Th17-associated cytokines *Il17a* and *Il17f*, (Figures 2A and 2B, middle panel), transcription factor (*Rorc*), and chemokines (*Ccl20* and *Ccr6*; Figure S2), reinforcing the prominent Th17 signature we observed by immunophenotyping, (Table S1). Expression of *Il22*, another major Th17-associated cytokine, was not detected in the majority (80%) of samples and was not different between groups (Figure S2). In contrast, colonized mice demonstrated lower levels of gap-junction-associated gene transcripts, which may represent increased epithelial permeability in colonized mice resulting from immune activation (Figures 2A and 2B, bottom panel; Table S1). We additionally examined genes associated with T helper cell effector functions. We observed increases in transcriptional signatures of Th1 (*Ifng*

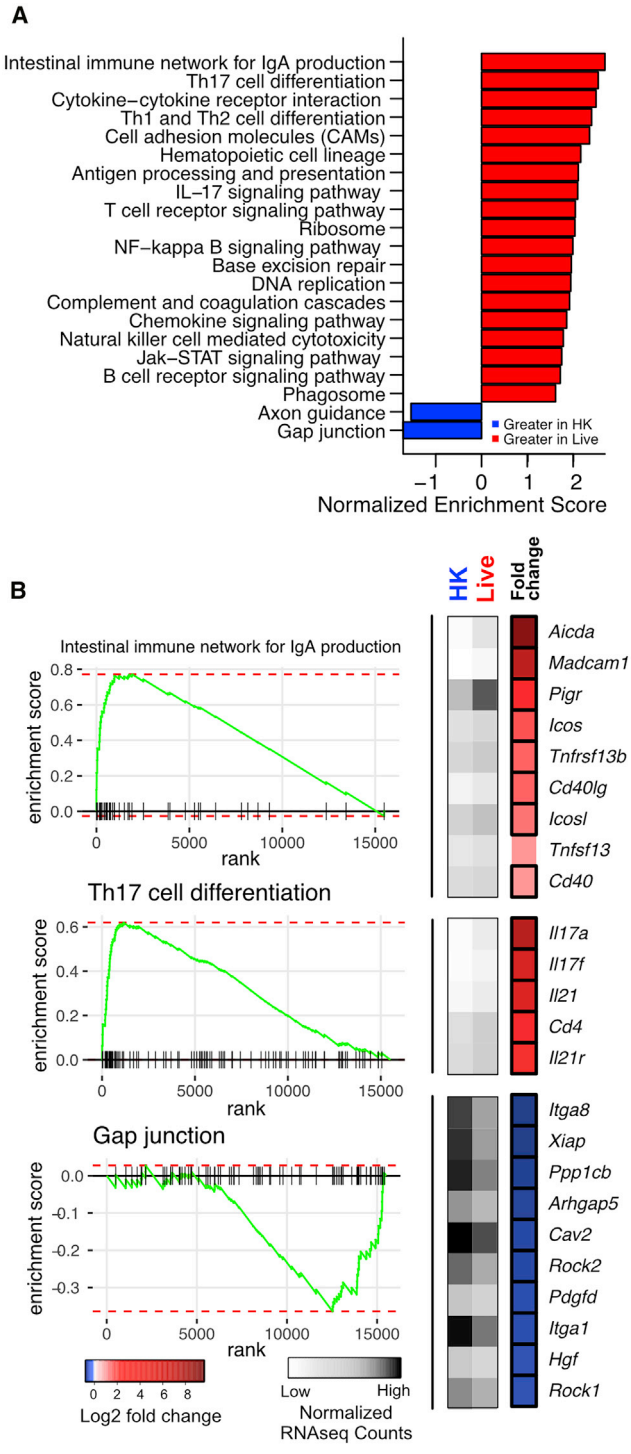

Figure 2. Host Transcriptomic Changes Due to *Bph* Colonization

(A) GSEA of KEGG pathways using whole-lung RNA-seq data from mice that received either live or HK *Bph* 52 days after inoculation. Only pathways with an adjusted p value of <0.05 are shown with their normalized enrichment score. Analysis was performed in R using the fgsea (Sergushichev, 2016) package. n = 5/group.

(B) Heatmaps and enrichment plots of selected KEGG pathways. On the left, enrichment plots for representative KEGG pathways are shown. To the right of each panel is a heatmap demonstrating normalized read counts and fold change of select leading-edge genes from each KEGG pathway. Average normalized read counts for HK (left column) and live (middle column) groups are shown in gray, and $\log_2$-fold change of each gene is shown in the rightmost column in blue and red. Genes that are significantly enriched are boxed. Analysis was performed in R using DEseq2.

Statistical significance: GSEA statistic as implemented in fgsea (Sergushichev, 2016) (A) or the Wald test with Benjamini-Hochberg (BH) correction as implemented in DESeq2 in (B).

and *Tbx21*) and Treg (*Foxp3*) cells but did not observe significant transcriptional changes in Th2-related genes (*Il4*, *Il5*, and *Il13*; Figure S2; Table S1).

In order to establish whether the expansion of Th17 cells to *Bph* was mediated by recognition of bacterial antigens displayed by antigen-presenting cells, we restimulated splenocytes from mice nasally inoculated with either HK or live *Bph*, stained them with carboxyfluorescein succinimidyl ester (CFSE), and then evaluated for cell division 72 h later. We observed an increase in the proliferation of activated T cells ($CFSE^{lo}CD25^{+}$) when splenocytes isolated from mice colonized with live bacteria were co-incubated with *Bph* lysate compared to when splenocytes from mice that received a HK inoculum were co-incubated with *Bph* lysate (Figure 3A, bottom versus top rows). Co-incubation of cultures with an anti-major histocompatibility complex class II (MHC II) antibody blocked $CD4^{+}$ T cell proliferation, confirming that *Bph* antigen requires MHC II to induce T cell proliferation (Figure 3A). Furthermore, ELISA quantification of IL-17A from the supernatants of restimulated cells from the lung demonstrated that $CD4^{+}$ T cells from *Bph*-colonized mice produced IL-17A in an antigen- and MHC-class-II-dependent manner (Figure 3B). IL-17A was not detectable in the supernatant of T cell cultures from control mice.

To further investigate the importance of an adaptive immune response in controlling bacterial abundance in the airways, we colonized WT and $RAG1^{-/-}$ C57BL/6J mice with *Bph* for 14 days and then sacrificed mice to assess the numbers of bacteria within bronchoalveolar lavage (BAL) fluid. We found that there was significantly greater *Bph* in the BALs of $RAG1^{-/-}$ than that of WT mice (Dewan et al., 2019), implicating an adaptive immune response in controlling the degree of bacterial colonization (Figure 3C). Interestingly, $RAG1^{-/-}$ mice colonized for 1 month with *Bph* did not demonstrate overt pneumonia (e.g., alveolar infiltrates) by histology (Figure S3A), nor significant weight loss compared to control mice that received a HK inoculum (Figure S3B), indicating that although an adaptive immune response helped control bacterial numbers, innate immune mechanisms were sufficient to prevent lethality. To further investigate the role of IL-17A in controlling *Bph* colonization, we treated mice with an anti-IL-17A blocking antibody before and during colonization (Figure 3D, top panel). Consistent with an important role for Th17 cells during *Bph* colonization, we found that mice treated with an anti-IL-17A blocking antibody had significantly higher titers of bacteria within the BAL and lung tissue than mice treated with an isotype control antibody (Figure 3D, bottom panel). Similar to $RAG1^{-/-}$ mice, although IL-17A aided in controlling *Bph* numbers, its blockade did not result in systemic effects, such as weight loss (Figure S3C).

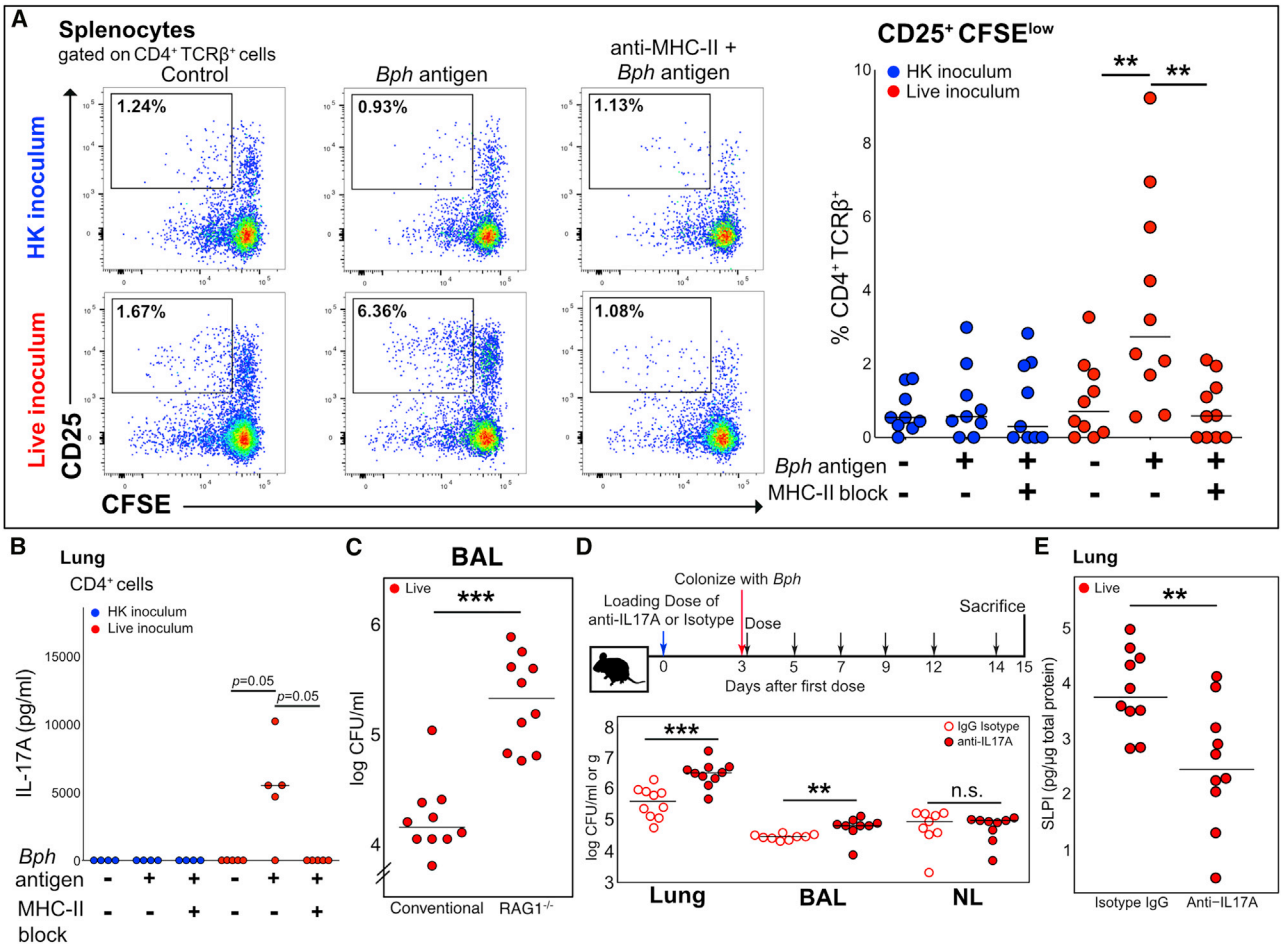

Figure 3. The Th17 Response to *Bph* Is Antigen Specific and Aids Controlling Colonization

(A) Left panel: Concatenated flow cytometry plots of cultures of splenocytes of five mice taken 52 days after inoculation with either HK or live *Bph*. Splenocytes were loaded with either no protein or *Bph* proteins from a HK culture. Cells were gated on $CD4^+TCR\beta^+$ cells using CD25 as an activation marker and CFSE as a proliferation marker. Representative of 2 independent experiments. Right panel: Quantification of $CD25^+CFSE^{lo}$ T cells from splenocyte cultures as shown in (A). n = 9–10 mice/group, combined from 2 independent experiments.

(B) IL-17A ELISA of culture supernatants from lung $CD4^+$ T cells co-cultured with antigen-loaded $CD11c^+$ dendritic cells (DCs). $CD4^+$ T cells were isolated from the lungs of five mice taken 43 days after inoculation with either HK or live *Bph*.

(C) CFU of *Bph* recovered from BALs of WT or $RAG1^{-/-}$ mice 14 days after colonization. n = 10 mice/group, combined from 2 independent experiments.

(D) Top: Schematic of the experimental approach to test the role of IL-17A during *Bph* colonization. Bottom: CFU of *Bph* recovered from lung homogenates (CFU/g), BAL, or nasal lavage (CFU/ml).

(E) ELISA showing SLPI protein expression in the lungs of mice inoculated with *Bph* and treated with anti-IL-17A monoclonal antibody compared to the isotype control.

Statistical significance: Kruskal-Wallis followed by post hoc one-tailed paired Wilcoxon rank-sum test with adjustment for multiple hypotheses using BH correction for (A) and (B) or two-tailed Wilcoxon rank-sum test for (C)–(E). Horizontal lines indicate median values. $^{**}p < 0.01$; $^{***}p < 0.001$.

Colonization with *Bph* Reduces Signatures of AAI

We next sought to test how long-term colonization with *Bph* and the Th17 response that it evokes would affect a concurrent allergic inflammatory response. To accomplish this, we colonized mice with *Bph* for 1 month before sensitizing and intranasally challenging mice to ovalbumin (OVA) (Figure 4A). Characterization of whole-lung tissue by flow cytometry demonstrated multiple alterations in immune cell populations that were attributable to *Bph* colonization. As previously seen in *Bph*-colonized mice (Figure 1), we noted an increased percentage of Teff populations (Figure S4A) and Th17 cells (Figure 4B) in mice undergoing OVA sensitization and challenge (OSC). However, in contrast to mice undergoing colonization alone, the percentage of Treg cells was reduced in colonized mice experiencing AAI (Figure S4B), and we noted no difference in neutrophils (Figure S4C).

We gauged the effect of *Bph* on AAI by assessing airway hyperresponsiveness (AHR), a characteristic feature of asthma, in colonized and control mice during methacholine challenge. Colonized mice demonstrated less airway resistance in response to methacholine challenge at 6.25 mg/ml and higher doses, indicating reduced AHR in mice with *Bph* compared to that in control mice (Figure 4C). These changes in resistance

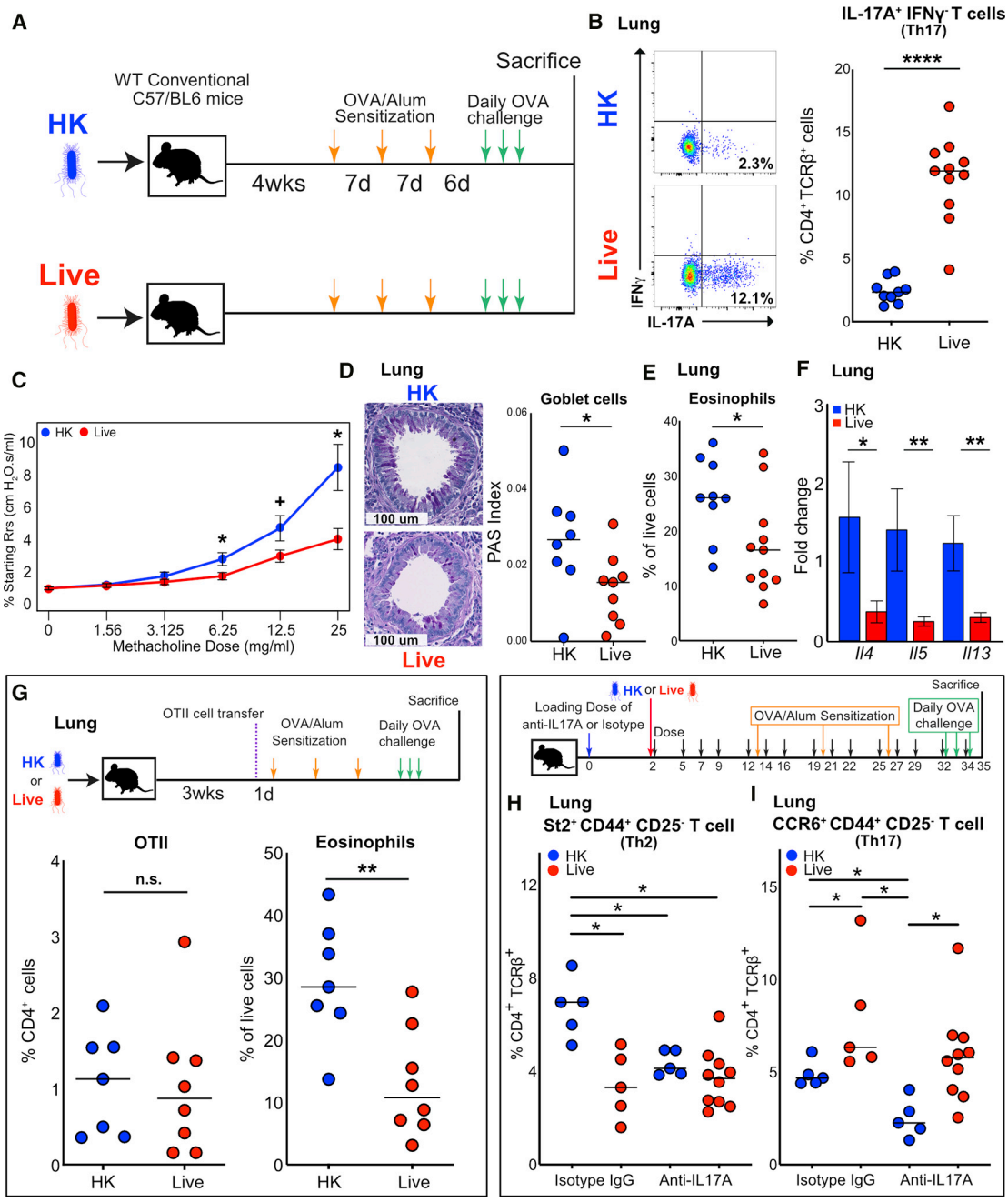

Figure 4. *Bph* Protects from Allergic Airway Inflammation in an Ovalbumin Model

(A) Schematic of the model to test the role of *Bph* in modulating AAI. Mice were inoculated with either HK or live *Bph* 4 weeks before starting OSC.

(B) Quantification of flow cytometry for intracellular cytokine staining of IL-17A$^+$IFNγ$^-$ CD4$^+$ T cells. n = 9–11 mice/group, combined from 2 independent experiments.

(C) Measurement of airway resistance in mice undergoing methacholine challenge after inducing AAI as shown in (A). Experiments were performed using a Flexivent FX1 system. Points represent mean ± SEM, n = 8 mice/group.

(D) Left: Representative PAS staining of mouse airways in mice initially receiving either an HK or live inoculum and then undergoing OSC. Right: Quantification of PAS-positive cells normalized to total bronchial epithelial area. n = 8–9 mice/group, combined from 2 independent experiments.

(E) Eosinophils as a percentage of live cells from lung. Eosinophils were defined as Ly6G$^-$CD11b$^+$SiglecF$^+$MHC II$^-$CD11c$^-$SSC^{hi} cells. n = 9–11 mice/group, combined from 2 independent experiments.

(F) qRT-PCR of whole-lung RNA from mice undergoing OSC. Bars represent mean ± SEM, n = 7–8 mice/group.

(legend continued on next page)

were also associated with reduced elastance and tissue damping, consistent with decreased AAI in control mice (Figure S4D). We also examined the effects of *Bph* colonization on allergic inflammatory markers. Periodic-acid-Schiff (PAS) staining, which identifies goblet cells, of OVA-challenged mice demonstrated that colonized animals had fewer goblet cells, indicating reduced goblet cell metaplasia (Figure 4D). Likewise, an analysis of whole-lung tissue showed that eosinophils, a marker for allergic inflammation and severity in mouse models, were reduced by ~38% in control compared to those of colonized mice (Figure 4E). Both eosinophil recruitment and goblet cell metaplasia are mediated by cytokines produced by Th2 cells, including IL-4, IL-5, and IL-13. Quantitative RT-PCR (qRT-PCR) of these cytokines confirmed that *Il4*, *Il5*, and *Il13* transcripts were reduced in OVA-sensitized and -challenged animals colonized with live *Bph* compared to those of HK controls (Figure 4F).

We next wanted to assess if the increased Th17 cells we observed in *Bph*-colonized, OVA-challenged mice represented bacterial-specific Th17 cells or if colonization created an environment that enhanced the generation of Th17 cells specific to OVA. As we observed in mice not exposed to OVA, splenocytes from colonized mice proliferated when stimulated with *Bph* lysates compared to those from mice exposed to a HK inoculum (Figure S3D). Similarly, restimulation of $CD4^+$ T cells isolated from the lung also proliferated in response to *Bph* lysates, showing that *Bph*-specific T cells persisted in the lungs of colonized mice undergoing OSC (Figure S3E). The Th17 response that we observed in colonized mice was also selective to *Bph* compared to other related bacteria within the same phylum, as we did not observe any proliferation of T cells (Figure S3E) and detected only a minimal production of IL-17A in response to restimulation with another Proteobacterium, *Escherichia coli* (Figure S3F).

Exposure to *Bph* lysates also resulted in the production of IL-17A from $CD4^+$ T cells isolated from the lung, spleen, mediastinal lymph node, and mesenteric lymph node of colonized mice. In contrast, IL-17A production by $CD4^+$ T cells from control mice was markedly decreased compared to that from colonized mice, demonstrating that airway colonization resulted in the dissemination of *Bph*-specific, IL-17A-secreting T cells systemically (Figure S3G).

Given the persistence of a *Bph*-specific immune response during AAI, we wanted to assess whether a pre-existing immune response to an airway bacterium could reduce the degree of allergic sensitization to OVA and, consequently, prevent AAI. We first looked at the capacity of colonized and control mice to generate OVA-specific serum IgE after sensitization and challenge, by ELISA (Klaßen et al., 2017). We found that colonization with *Bph* did not significantly alter the amount of OVA-IgE in the serum compared to control mice (Figure S4I). We next examined the T cell response to OVA and found that both colonized and control mice responded similarly to the restimulation of splenocytes to OVA *in vitro*, demonstrating similar degrees of proliferation in response to OVA (Figures S4E and S4F). Furthermore, splenocytes from both colonized and control mice produced IL-17A in response to OVA, and although colonized mice produced slightly more IL-17A in response to restimulation, the baseline IL-17A production was also higher, suggesting that the difference between live and HK groups was not OVA dependent (Figure S4G). We observed a similar pattern of IL-17A production from $CD4^+$ T cells isolated from the lung and restimulated with OVA, supporting the idea that the increased Th17 cells we observed in colonized mice undergoing OSC were primarily directed against *Bph* (Figure S4H).

Concurrent colonization with *Bph* could also decrease OVA presentation within the lung during allergic airway challenge, potentially accounting for the observed reduction in AAI. To assess if pre-existing colonization with *Bph* reduced OVA presentation in the lung, we injected colonized and control mice with $CD45.1^+CD4^+$ T cells expressing an OVA-specific T cell receptor (OTII) before sensitizing and challenging mice with OVA (Figure 4G, top panel). Both colonized and control mice had similar percentages and numbers of OTII cells in the spleen, suggesting that colonization did not systemically alter the response to OVA (Figures S5A and S5B). In the lungs of colonized mice receiving OTII cells, we again observed reduced eosinophils (Figure 4G, right), but the quantity of OTII T cells recruited to the lung was no different between colonized and control mice either by absolute counts (Figure S5C) or as a percentage of $CD4^+$ T cells (Figure 4G, left). Thus, the antigen presentation of OVA was likely to be similar regardless of colonization status.

To directly assess the contribution of IL-17A to AAI, we treated groups of either *Bph*-colonized or control mice with anti-IL-17A antibody or isotype control, starting at the time of colonization and extending throughout OSC (Figures 4H and 4I, top panel). At the conclusion of the experiment, mice receiving both live *Bph* and anti-IL-17A antibody had increased titers of *Bph* from their BALs, but not nasal lavages, compared to mice receiving an isotype control antibody (Figures S5D and S5E). Along with this increase in bacterial abundance, mice receiving both *Bph* and anti-IL-17A lost significantly more weight than mice receiving the isotype control antibody, regardless of colonization status (Figure S5F). The increases in bacterial abundance, as well as the weight loss observed in *Bph*-colonized mice receiving anti-IL-17A antibody, imply a protective role of IL-17A in *Bph*-colonized mice undergoing allergic airway sensitization and challenge.

To assess the effect of anti-IL-17A treatment on allergic inflammation in the lung, we performed flow cytometry on lung immune

(G) Top: Schematic of the experiment showing that mice were either inoculated with HK or live *Bph* 20 days before receiving 50,000 naive OTII T cells and then undergoing OSC. Bottom: Percentage of $CD4^+$ T cells ($CD4^+$) expressing the OT-II receptor ($CD45.1^+V\alpha2^+V\beta5^+$, left panel) and eosinophils as percentage of live cell (right panel) recruited to the lung. n = 7–8 mice/group, combined from 2 independent experiments.
(H) Top: Schematic of mice inoculated with HK or live *Bph* receiving anti-IL-17A antibody or an isotype control during colonization and then OSC. Bottom: Percentage of Th2 cells (defined as $TCR\beta^+CD4^+CD25^-CD44^+St2^+$) as a percentage of $CD4^+$ T cells.
(I) Percentage of Th17 cells (defined as $TCR\beta^+CD4^+CD25^-CD44^+CCR6^+$) as a percentage of $CD4^+$ T cells. n = 5–10 mice/group.
Statistical significance: Mann-Whitney U test for (B), (E), and (G). Wilcoxon rank-sum test for (C), (D), and (F). Kruskal-Wallis test followed by post hoc Wilcoxon rank-sum test with adjustment for multiple hypotheses using BH correction in (H) and (I). Horizontal lines indicate median values. + $p < 0.1$; *$p < 0.05$; **$p < 0.01$; ***$p < 0.001$; ****$p < 0.0001$.

cells using St2 expressed on Teff (TCRβ$^+$CD4$^+$CD25$^-$CD44$^+$St2$^+$, referred to as Th2 cells hereafter; CD25 was used to exclude Treg cells expressing St2) as a marker for allergic inflammation. St2, or IL-33R, is known to be preferentially expressed on Th2 polarized cells (Löhning et al., 1998) and directly contributes to AAI by helping upregulate Th2 cytokine production (Schmitz et al., 2005). Affirming our earlier findings (Figures 4C–4F), we found that mice colonized with *Bph* and treated with the isotype control antibody had signs of reduced AAI, with lower percentages of Th2 cells than those of HK controls also receiving the isotype antibody (Figures 4H and S5G). Anti-IL-17A treatment reduced the severity of AAI, as measured by the percentage of Th2 cells in mice receiving a HK inoculum and treated with anti-IL-17A compared to isotype-control-antibody-treated mice. Blockade of IL-17A, however, did not significantly change the percentages of Th2 cells present in colonized mice, which were significantly reduced compared to isotype-treated HK mice.

To further understand these findings, we tested for differences in Th17 cells by examining Teff expressing CCR6, a marker for Th17 cells (Hirota et al., 2007) (TCRβ$^+$CD4$^+$CD25$^-$CD44$^+$CCR6$^+$; referred to as Th17 cells hereafter). As shown previously (Figures 1F and 4B), mice colonized with *Bph* had higher levels of Th17 cells than HK mice (Figures 4I and S5H). Anti-IL-17A treatment reduced percentages of Th17 cells in HK mice when compared to isotype-treated HK controls. Yet, in *Bph*-colonized animals, the anti-IL-17A treatment did not significantly alter the percentages of Th17 cells, suggesting that blockade of IL-17A is insufficient to reverse the protective effect of *Bph* colonization. Although the percentages of Th17 cells in *Bph*-colonized mice was not different between anti-IL-17A and isotype control, the increase in bacterial abundance in the airway may provoke a compensatory immune response that complicates our interpretation of the role of IL-17A in our model of AAI. These results support the idea that Th17 cells induced by *Bph* are associated with protection from AAI but that monoclonal antibodies targeting IL-17A are inadequate to reverse their effect on AAI.

SLPI Is Regulated by Airway Colonization

To better understand how *Bph* reduces susceptibility to AAI, we examined the lung tissue transcriptional profile of mice undergoing OSC. This analysis corroborated our observation that *Bph* colonization resulted in a reduction in multiple markers of allergic inflammation (see Table S2; Figures 4F and 5A). Notably, the effect on these Th2 markers was only apparent in mice undergoing AAI because we noted no differences in expression of Th2-related cytokines in mice not undergoing sensitization and challenge (Figure S2; Table S1). Similarly, GSEA only identified two Kyoto Encyclopedia of Genes and Genomes (KEGG) pathways that were significantly enriched in colonized mice undergoing OSC (Figures S6A and S6B), neither of which were enriched in colonized mice not undergoing AAI (Figure 2A). Examination of leading-edge genes from the IgA protection network and focal adhesion pathways identified in Figure 2A showed that these genes were no longer significantly different in mice undergoing OVA sensitization, consistent with the effects of AAI reducing the transcriptional signatures associated with colonization (Figure S6C).

To find genes mediating protection from AAI, we sought to identify transcripts that were upregulated in colonized compared to control animals, both in mice undergoing colonization only (Table S1) and in mice undergoing OSC (Table S2). This analysis revealed that 44 genes were upregulated in both datasets by a minimum of a 2-$\log_2$-fold change with a maximum p value of 0.05 after correction for multiple hypotheses (Figure 5B, triangles). A total of 16 of these 44 transcripts originated from genes involved in immune system processes (Figures 5A and 5B, blue triangles). In addition to genes involved in germinal center formation (*Nuggc*) and antibody biosynthesis (*Jchain*), we noted that *Slpi* was significantly upregulated by *Bph*. We confirmed that the transcriptional upregulation of *Slpi* was also accompanied by increased SLPI protein in the lungs of *Bph*-colonized mice undergoing OSC (Figure 5C).

Slpi was first characterized as a constitutively expressed inhibitor of neutrophil elastase in the lung and has been demonstrated to be an important antimicrobial peptide in the airway, with efficacy against both Gram-negative and Gram-positive bacteria (Hiemstra et al., 1996; Wiedow et al., 1998). Animal models have directly demonstrated that mice lacking *Slpi* experience worsened AAI (Marino et al., 2011) and that endogenously overexpressed (Raundhal et al., 2015) or exogenously administered SLPI (Forteza et al., 2001) can mitigate AAI, indicating that *Slpi* may play a protective role in asthma. Although *Slpi* is known to be upregulated by innate immune activation through the functions of tumor necrosis factor alpha (TNF-α) and IL-1β (Sallenave et al., 1994), we noted that SLPI protein levels correlated with *Il17a* transcription in the lungs of mice undergoing AAI and may help to mediate the reduction of AAI observed in *Bph*-colonized mice (Figure 5D).

To test the idea that colonization with *Bph* increases the expression of SLPI within the lung through IL-17A, we first used qPCR to establish that microbial colonization of mice modulates the expression of *Slpi* in the lung by comparing conventionally raised WT, RAG1$^{-/-}$, and germ-free (GF) C57BL/6 mice either undergoing 2 weeks of colonization with *Bph* or remaining non-colonized (Figure 5E). We first confirmed that the transcription of *Slpi* in WT mice was significantly upregulated in colonized mice compared to controls. In contrast, RAG1$^{-/-}$ mice did not demonstrate increased *Slpi* expression in response to *Bph* colonization, suggesting that the adaptive immune system helps regulate the expression of SLPI (Figure 5E). These results also showed that increased *Slpi* expression in the lung reflects local (rather than gut) microbial exposure since GF and non-colonized conventional mice had similar amounts of *Slpi* expression.

We next asked if the positive regulation of SLPI resulting from *Bph* colonization was mediated through IL-17A by treating a human lung epithelial cell line (A549) with TNF-α, IL-1β, and IL-17A. We found that although IL-1β and TNF-α alone were sufficient to upregulate *Slpi*, IL-17A did not significantly increase *Slpi*. Incubation of A549 cells with both TNF-α and IL-17A, however, demonstrated increased *Slpi* transcription in cells incubated with both cytokines compared to either one singly (Figure 5F). To confirm that IL-17A played a role in potentiating SLPI production *in vivo*, we examined mice colonized with *Bph* and treated them with a neutralizing monoclonal antibody to IL-17A for 2 weeks (Figure 3D). Compared to mice receiving an isotype control, colonized mice treated with an anti-IL-17A antibody showed reduced levels of SLPI in the lungs, as measured by

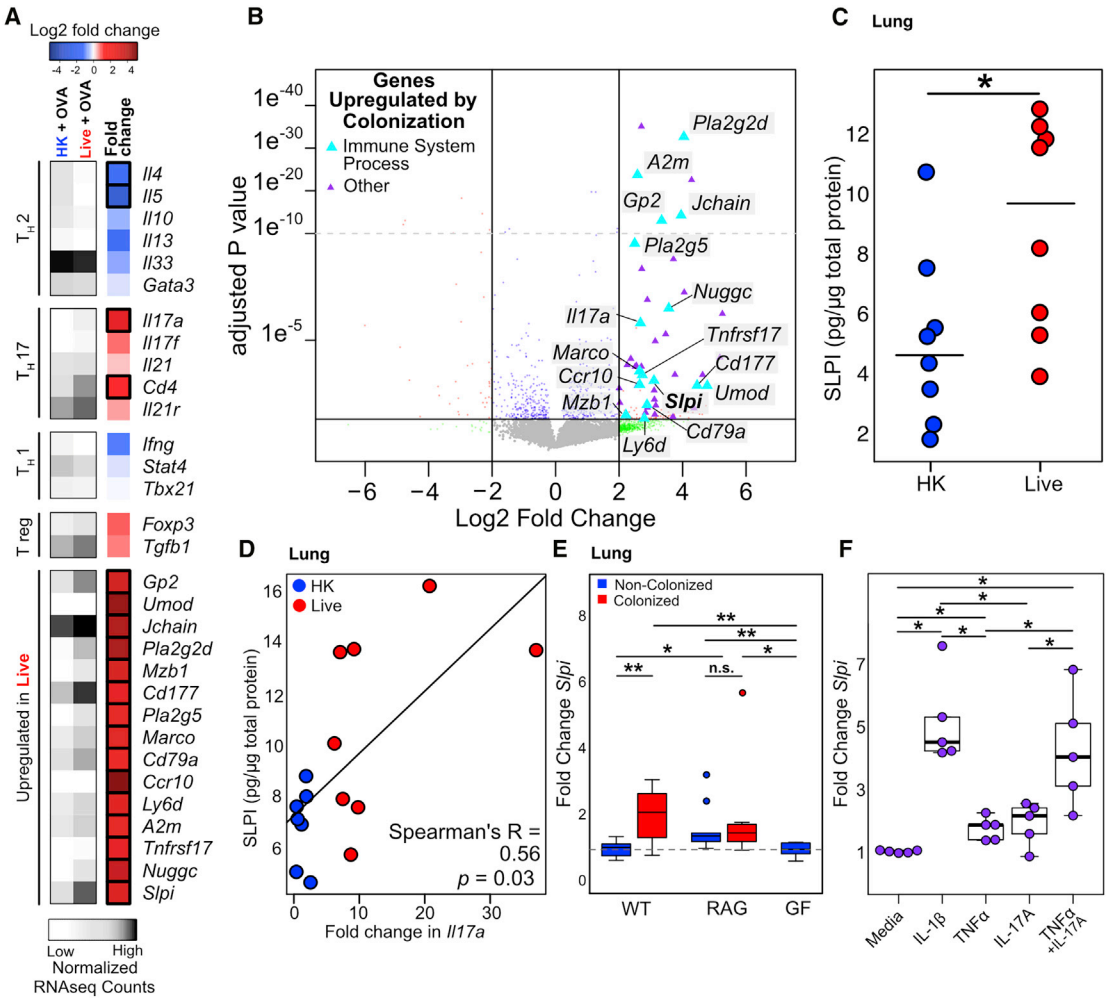

Figure 5. SLPI Is Regulated by Colonization and Mediates Protection from AAI

(A) Heatmap of immune genes regulated by *Bph* colonization in mice undergoing AAI. Average normalized read counts for each group are shown in gray, and $\log_2$-fold change in mice that received a live, compared to an HK, inoculum for each gene is shown in blue, white, and red. n = 3–5 mice/group.

(B) Volcano plot of whole-lung transcriptomic data from mice that received either an HK or live *Bph* inoculum and then underwent OSC (as shown in Figure 4A). Genes depicted as triangles were significantly enriched in colonized mice not undergoing AAI. Genes involved in an immune system process (defined by the Gene Ontogeny [GO] pathway, GO: 0002376) are shown in light blue and are also depicted in the heatmap shown in (A). n = 3–5 mice/group.

(C) ELISA showing SLPI protein expression in the lungs of mice inoculated with live *Bph* followed by AAI compared to those inoculated with HK. n = 7–8 mice/group.

(D) Correlation between SLPI protein expression and fold change in *Il17a* measured by qRT-PCR in the lungs of mice inoculated with HK or live *Bph*, followed by AAI. n = 7–8 mice/group

(E) qRT-PCR of SLPI from the whole lungs from germ-free, RAG1$^{-/-}$, and conventionally raised WT mice. n = 9–10 mice/group.

(F) Transcription of *Slpi* in human alveolar epithelial cell line A549 in response to cytokine stimulation. Cells were treated with 1 ng/ml IL-1β, 100 ng/ml IL-17A, and/or 10 ng/ml TNF-α as shown. Experiment performed in n = 5 biological replicates, each representing the average of 3 technical replicates.

Statistical significance: Wald test with BH correction as implemented in DESeq2 in (A) and (B); Wilcoxon rank-sum test for (C); Spearman's rank test in (D); or Kruskal-Wallis test followed by post hoc two-tailed paired Wilcoxon rank-sum test with adjustment for multiple hypotheses using BH correction in (E) and (F). Boxes indicate 25th and 75th percentiles and whiskers are 1.5 × interquartile range. *p < 0.05; **p < 0.01; ***p < 0.001; ****p < 0.0001.

ELISA (Figure 3E), supporting a stimulatory effect of IL-17A on SLPI production in the lung.

SLPI Shapes the Microbial Ecology of the Upper Airway in Humans

Our results demonstrate that SLPI is regulated by airway microbial colonization in mice and that higher amounts of SLPI are associated with reduced intensity of AAI we observe in *Bph*-colonized mice. In humans, lower expression of SLPI from epithelial brushings has previously been reported in individuals with severe asthma (Raundhal et al., 2015). To test the idea that microbial airway colonization could modulate the production of SLPI within the airway, we first selectively cultured nasal lavage specimens from adults and children with moderate to

Table 1. Recovery of *Haemophilus*, *Streptococcus*, and *Moraxella* from the Nasal Lavage of MARS Participants

	Adult and Pediatric				Adult				Pediatric			
Genus	Asthma (34)	Healthy (55)	p value	adjusted (adj.) p value	Asthma (16)	Healthy (35)	p value	adj. p value	Asthma (18)	Healthy (20)	p value	adj. p value
Haemophilus	76%	35%	0.00017*	0.0015*	50%	11%	0.0047*	0.021*	100%	75%	0.048*	0.14
Streptococcus	65%	49%	0.19	0.28	38%	31%	0.75	0.84	89%	80%	0.66	0.84
Moraxella	12%	2%	0.068	0.15	0%	0%	1	1	22%	5%	0.17	0.28

Statistical significance: Fisher's exact test with adjustment for multiple hypotheses using BH correction.
*Denotes significance.

severe asthma or healthy controls (from the Microbiota in Asthma Research Study [MARS]; see Table S3 for demographic data) for *Haemophilus*, *Streptococcus*, and *Moraxella* airway bacteria previously associated with asthma. Overall, we noted that children demonstrated higher recovery of *Haemophilus* and *Streptococcus* ($p < 0.0001$ for each comparison, Fisher's exact test) from nasal lavage than adults regardless of health status (Table 1). Consistent with prior reports of other respiratory microbiologic surveys in asthma (Bisgaard et al., 2007; Durack et al., 2017), we recovered *Haemophilus* more frequently from nasal lavages from adults and children with asthma than healthy controls (Table 1).

We did not observe any significant differences in nasal lavage SLPI abundances between healthy and asthmatic populations (Thijs et al., 2015; Figure S7A). However, we next performed an exploratory analysis to ask if nasal lavage SLPI corresponded with asthma control by comparing Asthma Control Test (ACT) scores, a clinically validated survey of symptom control in asthmatics (Nathan et al., 2004). This analysis showed that in adult asthmatics, better asthma control (corresponding to higher ACT scores) corresponded to higher nasal SLPI levels, consistent with a protective role for SLPI in asthma (Figure 6A). We also observed a relationship between SLPI and *Haemophilus* upper airway colonization across the adult and pediatric populations by showing a positive correlation between SLPI nasal concentration and the titers of *Haemophilus* recovered from colonized individuals (Figure 6B). These differences did not appear to be due to the amount of corticosteroid usage because we observed no difference in nasal SLPI levels in asthmatics between those with the highest inhaled corticosteroid doses and those with lower doses ($p = 0.8$, Wilcoxon rank-sum test; Table S3).

Together, these results show that SLPI abundance in the nasal passages is correlated both with the presence of *Haemophilus* and a clinical correlate of asthma control. Although SLPI levels in the airway are known to be modulated by bacterial colonization and infection (Parameswaran et al., 2011), we hypothesized that airway microbial community composition, as a whole, would also influence SLPI abundance. To test a relationship between SLPI levels and microbial community composition, we quantified SLPI and performed V4-16S rRNA sequencing on oral lavage samples from MARS participants. Similar to the nasal lavage specimens, we did not observe a difference in SLPI from oral lavage specimens (Figure S7B). 16S rRNA analysis showed that the composition of these oral microbial communities was consistent with prior surveys of oral microbial communities (Aas et al., 2005), showing that these communities were made up largely of *Streptococcus*, *Veillonella*, and *Prevotella* species (Figure S7C). We did not discern any differences in alpha diversity (Figure S7D) nor community composition (Figure S7E) in the microbial ecology of oral lavage specimens between the different cohorts. To test the idea that SLPI abundances in oral lavage samples would reflect microbial community composition, we built a supervised learning model from healthy adults and children ($n = 55$) to predict oral SLPI levels based on 16S rRNA abundance data. We first identified 11 taxa (Figure 6D) that were important for predicting SLPI abundances using random forest (Liaw and Wiener, 2002). These taxa were used to build a model that explained 40% of the variance in the oral lavage SLPI levels measured by ELISA (Figure 6C). This correlation was maintained after a 10-fold cross-validation, indicating that overfitting plays a limited role in the success of the model (Figure 6C, inset). Of the 11 taxa that we included in our model (Figure 6D), some of these bacteria or their close relatives have previously been noted to elicit, or be susceptible to, SLPI *in vitro* (e.g., *Neisseria*; Cooper et al., 2012).

DISCUSSION

Asthma is known to be shaped by a myriad of genetic factors, environmental factors, and—increasingly—microbial exposures. Although components of the airway microbiota have been previously associated with enhanced susceptibility to asthma, our findings point to a complex and potentially beneficial role of some bacteria within the airway. In this study, we show that airway colonization of mice with *Bph*, a murine-adapted bacterium, elicits a Th17 immune response that aids in controlling bacterial abundance in the airway. Furthermore, we show that when animals undergo AAI challenge, mice previously colonized with *Bph* demonstrate protection from AAI. Colonization with *Bph* does not appear to impact the degree of allergic sensitization nor the presentation of allergen in the lung, but our results do suggest an effect of colonization on Th2 polarization and blunting of allergic effector cell recruitment. In contrast to other studies that have emphasized the potentially deleterious roles of allergen-specific T cells polarized to Th17 in AAI (McKinley et al., 2008; Wakashin et al., 2008), our results show that immune responses to airway bacteria co-exist with immune responses to allergens and could counteract allergic responses. Although we were unable to demonstrate a direct protective role of IL-17A induced by *Bph*, this could be explained in part by the dual effect of anti-IL-17A on both bacterial colonization and AAI. Because anti-IL-17A treatment results in increased *Bph* titers, this worsened infection may offset the effects of IL-17A blockade by

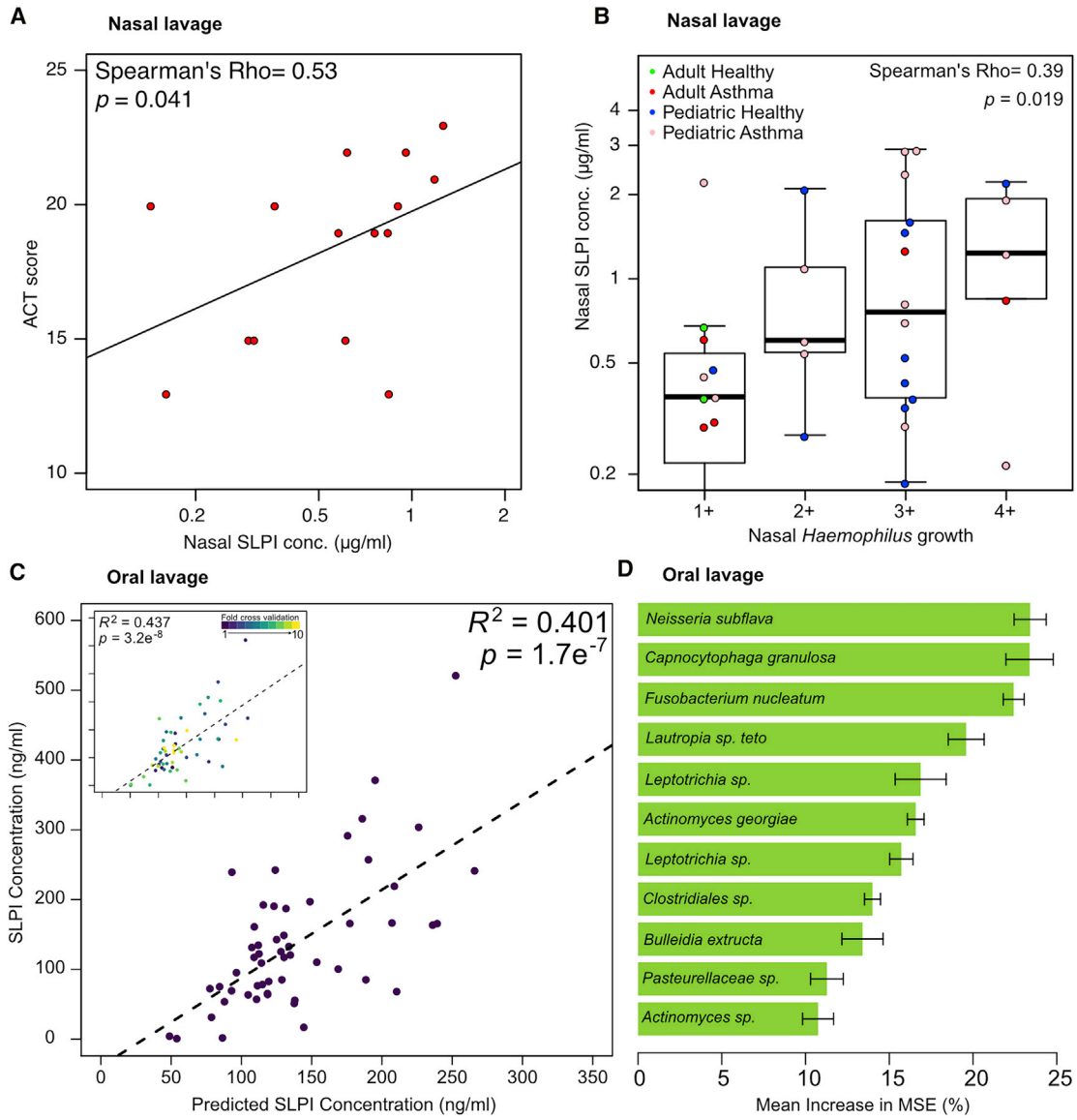

Figure 6. SLPI Levels in Human Upper Airways Are Regulated by the Microbiota

(A) Correlation of ACT score to nasal lavage SLPI from adult asthmatics.

(B) Correlation of SLPI to recovery of *Haemophilus* in nasal lavage fluid. All individuals with and without asthma from both adult and pediatric cohorts that had *Haemophilus* colonization were included in this analysis.

(C) Oral lavage microbial community composition predicts SLPI levels. V4-16S data from healthy human children and adults were used to construct a Random Forest model to predict SLPI levels based on the abundance of 11 amplicon sequence variants (ASVs). Ten-fold cross-validation of this model performed comparably to the complete model (inset).

(D) The taxonomic assignments and mean increase in mean square error (MSE) of ASVs included in the Random Forest model depicted in (C). The mean increase in MSE is an estimate of the importance of each taxon to the Random Forest model.

Statistical significance: Spearman's rank-order correlation for (A) and (B); or Pearson's correlation in (C). Boxes indicate 25th and 75th percentiles and whiskers are 1.5 × interquartile range.

further stimulating a bacterial Th17 immune response, which is consistent with our observation that Th17 cells were not reduced in colonized mice treated with anti-IL-17A (Figure 4I). Alternatively, recent advances have shown that blocking IL-17A may lead to a compensatory upregulation of other Th17-related cytokines in some types of Th17 cells, which could also mitigate the effects of anti-IL-17A antibodies (Chong et al., 2020). Together, our data support previously described protective roles for Th17 in blunting allergic effector responses (Schnyder-Candrian et al., 2006) but additionally implicate immune responses to airway commensals as a potential source for this Th17 response.

During *Bph* colonization, we observed that the Th17 response was associated with increased expression of antimicrobial peptides, including SLPI, in the lung. Although SLPI is known to be regulated by TNF-α and IL-1β (Sallenave et al., 1994), we show that its expression is enhanced by IL-17A *in vitro* and *in vivo*. The potential of SLPI to mitigate AAI has been appreciated for decades (Wright et al., 1999), and low SLPI airway levels have been previously noted in severe asthma (Raundhal et al., 2015). A direct protective role of SLPI in AAI has been shown in animal models demonstrating that mice lacking SLPI have increased Th2 polarization markers, increased eosinophil recruitment, and worsened measures of AHR (Marino et al., 2011). The molecular and cellular targets of SLPI still require additional investigation. SLPI is known to have the ability to directly penetrate cells to inhibit nuclear factor κB (NF-κB) signaling (Taggart et al., 2005), and exogenously administered SLPI (Wright et al., 1999), as well as SLPI expressed from a transgene (Marino et al., 2011; Raundhal et al., 2015), reduces eosinophilic inflammation in models of AAI. Additionally, SLPI has been demonstrated to be an endogenous regulator of eosinophil and basophil function by inhibiting Toll-like receptor 4 (TLR4) signaling in allergic inflammation (Matsuba et al., 2017). However, more studies investigating the tissue-specific effects of SLPI resulting from airway bacterial colonization will be needed to address which cell types and molecular targets are affected by SLPI and mediate protection from AAI. Along with our findings that SLPI shapes upper airway microbial ecology and is enhanced by IL-17A, this suggests an important role for Th17 responses in regulating airway microbiota composition that may, in turn, affect AAI severity.

Our results help improve our understanding of the nature of airway microbe-immune interactions in human asthma and could have clinical ramifications. IL-17A and its associated effector functions, such as neutrophilia, are currently being investigated as both biomarkers for particular asthma endotypes and therapeutic targets. However, preliminary studies targeting IL-17A in asthma have not proven to be uniformly efficacious, potentially indicating varied roles of Th17 responses in asthma. Our findings directly demonstrate that although a blockade of IL-17A reduced markers of AAI in non-colonized mice, this protective response was lost upon bacterial airway colonization with *Bph*. This microbiota-mediated variability in response to anti-IL-17A therapy could be clinically relevant as better understanding the interplay between airway microbes and AAI could help define individuals that are likely to benefit from IL-17A-targeted therapies.

In our clinical study, we observed an increased prevalence of colonization with *Haemophilus* in asthmatics in both our pediatric and adult cohorts. Interestingly, the quantity of SLPI was associated both with individual bacteria in nasal specimens and overall microbial community composition from oral lavages. Combined with observations that SLPI abundance in the airway is modulated during infection (Parameswaran et al., 2011; Persson et al., 2017), we propose that regulation of SLPI expression is a crucial mechanism underlying homeostasis between the respiratory microbiota and the airway mucosal immune system. In addition to its correlation to *Haemophilus* in the upper airway, SLPI tended to be lower in adult subjects with poor asthma control. Although our finding that SLPI levels were increased with *Haemophilus* abundance may seem at odds with the previously described role of *Haemophilus* in severe asthma (Goleva et al., 2013; Simpson et al., 2016), we note that the correlation between SLPI and *Haemophilus* included both healthy and asthmatic individuals. One interpretation of our data is that the relationship between SLPI and *Haemophilus* may differ between healthy and asthmatic individuals, as evidenced by the ability of *Haemophilus* to alter the behavior of the immune system in the context of airway inflammation (Shilts et al., 2020). Furthermore, patients from the MARS study were limited to those with moderate to severe asthma without an ongoing exacerbation and do not represent the entire spectrum of asthma phenotypes and *Haemophilus* colonization. Nevertheless, our data suggest that SLPI expression is part of a regulatory response associated with *Haemophilus* colonization and that appropriate expression in the context of airway colonization is part of a beneficial response that leads to better controlled asthma.

A potential limitation of our study is that *Bph* itself is not a known human airway colonizer. Although other members of the *Bordetella* genus can colonize the airways, their relationship to asthma is less well characterized than HSM organisms. Nevertheless, in contrast to human airway microbes, the persistent colonization of *Bph* in the airways without inducing an overt pneumonia, combined with its potent ability to alter immunity, offers a perspective of respiratory bacteria as potentially beneficial, rather than detrimental, in asthma. *Bph*'s unique adaptation to the murine airway could make it a powerful tool to advance our understanding of airway microbe-immune interactions important in respiratory inflammatory diseases. An additional limitation from our human study was that we only observed a correlation between SLPI and asthma control in our adult cohort. This could be the result of the small sample size or differences in asthma control between our adult and pediatric cohorts (adults tended to have poorer asthma control), or it could indicate differences in the immune responses associated with asthma between adult and pediatric populations. In addition to addressing the role of SLPI in pediatric populations, future human studies will be needed to confirm the relationship between upper airway microbial ecology and SLPI using culture-independent methods and to determine the specific immune signatures, such as IL-17A, associated with SLPI production in asthma.

Overall, our findings support a key role of airway microbes in shaping the severity and character of AAI responses. In the context of our increasing recognition of asthma as a clinically and immunologically heterogeneous disease, our results emphasize the importance of taking the resident airway microbiota into account when evaluating immune responses in the context of asthma. Differentiating Th17 responses directed against exogenous allergens versus those directed at colonizing airway bacteria may prove to have an important impact on how we interpret the role of Th17 responses in asthma. We propose that SLPI's multifactorial role as a microbiota-responsive, immune-modulatory protein makes it a biomarker for dissecting the relationships between airway microbial communities and asthma.

STAR★METHODS

Detailed methods are provided in the online version of this paper and include the following:

SUPPLEMENTAL INFORMATION

Supplemental Information can be found online at https://doi.org/10.1016/j.celrep.2020.108331.

ACKNOWLEDGMENTS

We thank Tarisa Mantia, Caitlin O'Shaughnessy, and Shannon Rook for their assistance with patient recruitment and members of the Kau lab for helpful discussions. We would also like to thank MARS study participants and their families. The research was supported by the AAAAI Foundation Faculty Development Award (to A.L.K.), the American Asthma Foundation (to C.-S.H. and A.L.K.), and NIH grants T32 GM007200 (to A.L.R.), R01 AI136515 (to C.-S.H.) and K08 AI113184 (to A.L.K.).

AUTHOR CONTRIBUTIONS

Investigation, N.J., R.T.M., A.L.R., A.H.-L., N.G.W., M.A.L., E.V.R.-G., J.N.C., and A.L.K. Conceptualization, N.J., R.T.M., A.L.R., L.B.B., C.-S.H., and A.L.K. Formal Analysis, N.J., A.L.R., A.H.-L., N.G.W., and A.L.K. Software, A.L.R, A.H.-L., N.G.W., and A.L.K. Visualization, N.J. and A.L.R. Writing – Original Draft, N.J. and A.L.K. Writing - Review & Editing, N.J., R.T.M., A.L.R., A.H.-L., N.G.W., L.B.B., C.-S.H., and A.L.K. Funding Acquisition, C.-S.H. and A.L.K.

DECLARATION OF INTERESTS

The authors declare no competing interests.

Received: February 21, 2020
Revised: August 22, 2020
Accepted: October 8, 2020
Published: November 3, 2020

REFERENCES

Aas, J.A., Paster, B.J., Stokes, L.N., Olsen, I., and Dewhirst, F.E. (2005). Defining the normal bacterial flora of the oral cavity. J. Clin. Microbiol. *43*, 5721–5732.

Allen, E.K., Pitkäranta, A., Mäki, M., Hendley, J.O., Laakso, S., Sale, M.M., and Winther, B. (2013). Bacteria in the nose of young adults during wellness and rhinovirus colds: detection by culture and microarray methods in 100 nasal lavage specimens. Int. Forum Allergy Rhinol. *3*, 731–739.

Alnahas, S., Hagner, S., Raifer, H., Kilic, A., Gasteiger, G., Mutters, R., Hellhund, A., Prinz, I., Pinkenburg, O., Visekruna, A., et al. (2017). IL-17 and TNF-α Are Key Mediators of *Moraxella catarrhalis* Triggered Exacerbation of Allergic Airway Inflammation. Front. Immunol. *8*, 1562.

Altschul, S.F., Gish, W., Miller, W., Myers, E.W., and Lipman, D.J. (1990). Basic local alignment search tool. J. Mol. Biol. *215*, 403–410.

Amezcua Vesely, M.C., Pallis, P., Bielecki, P., Low, J.S., Zhao, J., Harman, C.C.D., Kroehling, L., Jackson, R., Bailis, W., Licona-Limon, P., et al. (2019). Effector TH17 Cells Give Rise to Long-Lived TRM Cells that Are Essential for an Immediate Response against Bacterial Infection. Cell *178*, 1176–1188.e1115.

Anders, S., Pyl, P.T., and Huber, W. (2015). HTSeq—a Python framework to work with high-throughput sequencing data. Bioinformatics *31*, 166–169.

Bankevich, A., Nurk, S., Antipov, D., Gurevich, A.A., Dvorkin, M., Kulikov, A.S., Lesin, V.M., Nikolenko, S.I., Pham, S., Prjibelski, A.D., et al. (2012). SPAdes: a new genome assembly algorithm and its applications to single-cell sequencing. J. Comput. Biol. *19*, 455–477.

Barlow, J.L., Flynn, R.J., Ballantyne, S.J., and McKenzie, A.N. (2011). Reciprocal expression of IL-25 and IL-17A is important for allergic airways hyperreactivity. Clin. Exp. Allergy *41*, 1447–1455.

Beura, L.K., Hamilton, S.E., Bi, K., Schenkel, J.M., Odumade, O.A., Casey, K.A., Thompson, E.A., Fraser, K.A., Rosato, P.C., Filali-Mouhim, A., et al. (2016). Normalizing the environment recapitulates adult human immune traits in laboratory mice. Nature *532*, 512–516.

Bisgaard, H., Hermansen, M.N., Buchvald, F., Loland, L., Halkjaer, L.B., Bønnelykke, K., Brasholt, M., Heltberg, A., Vissing, N.H., Thorsen, S.V., et al. (2007). Childhood asthma after bacterial colonization of the airway in neonates. N. Engl. J. Med. *357*, 1487–1495.

Bisgaard, H., Hermansen, M.N., Bønnelykke, K., Stokholm, J., Baty, F., Skytt, N.L., Aniscenko, J., Kebadze, T., and Johnston, S.L. (2010). Association of bacteria and viruses with wheezy episodes in young children: prospective birth cohort study. BMJ *341*, c4978.

Callahan, B.J., McMurdie, P.J., Rosen, M.J., Han, A.W., Johnson, A.J., and Holmes, S.P. (2016). DADA2: High-resolution sample inference from Illumina amplicon data. Nat. Methods *13*, 581–583.

Caporaso, J.G., Lauber, C.L., Walters, W.A., Berg-Lyons, D., Lozupone, C.A., Turnbaugh, P.J., Fierer, N., and Knight, R. (2011). Global patterns of 16S rRNA diversity at a depth of millions of sequences per sample. Proc. Natl. Acad. Sci. USA *108*, 4516–4522.

Chen, K., McAleer, J.P., Lin, Y., Paterson, D.L., Zheng, M., Alcorn, J.F., Weaver, C.T., and Kolls, J.K. (2011). Th17 cells mediate clade-specific, serotype-independent mucosal immunity. Immunity *35*, 997–1009.

Chen, S.L., Wu, M., Henderson, J.P., Hooton, T.M., Hibbing, M.E., Hultgren, S.J., and Gordon, J.I. (2013). Genomic diversity and fitness of E. coli strains recovered from the intestinal and urinary tracts of women with recurrent urinary tract infection. Sci. Transl. Med. *5*, 184ra60.

Chen, L., Zheng, D., Liu, B., Yang, J., and Jin, Q. (2016). VFDB 2016: hierarchical and refined dataset for big data analysis–10 years on. Nucleic Acids Res. *44*, D694–D697.

Chesné, J., Braza, F., Mahay, G., Brouard, S., Aronica, M., and Magnan, A. (2014). IL-17 in severe asthma. Where do we stand? Am. J. Respir. Crit. Care Med. *190*, 1094–1101.

Chong, W.P., Mattapallil, M.J., Raychaudhuri, K., Bing, S.J., Wu, S., Zhong, Y., Wang, W., Chen, Z., Silver, P.B., Jittayasothorn, Y., et al. (2020). The Cytokine

IL-17A Limits Th17 Pathogenicity via a Negative Feedback Loop Driven by Autocrine Induction of IL-24. Immunity *53*, 384–397.e385.

Choy, D.F., Hart, K.M., Borthwick, L.A., Shikotra, A., Nagarkar, D.R., Siddiqui, S., Jia, G., Ohri, C.M., Doran, E., Vannella, K.M., et al. (2015). TH2 and TH17 inflammatory pathways are reciprocally regulated in asthma. Sci. Transl. Med. *7*, 301ra129-301ra129.

Clark, S.E., Purcell, J.E., Sammani, S., Steffen, E.K., Crim, M.J., Livingston, R.S., Besch-Williford, C., and Fortman, J.D. (2016). Bordetella pseudohinzii as a Confounding Organism in Murine Models of Pulmonary Disease. Comp. Med. *66*, 361–366.

Clark, S.E., Purcell, J.E., Bi, X., and Fortman, J.D. (2017). Cross-Foster Rederivation Compared with Antibiotic Administration in the Drinking Water to Eradicate *Bordetella pseudohinzii*. J. Am. Assoc. Lab. Anim. Sci. *56*, 47–51.

Cooper, M.D., Roberts, M.H., Barauskas, O.L., and Jarvis, G.A. (2012). Secretory leukocyte protease inhibitor binds to Neisseria gonorrhoeae outer membrane opacity protein and is bactericidal. Am. J. Reprod. Immunol. *68*, 116–127.

Dewan, K.K., Taylor-Mulneix, D.L., Campos, L.L., Skarlupka, A.L., Wagner, S.M., Ryman, V.E., Gestal, M.C., Ma, L., Blas-Machado, U., Faddis, B.T., and Harvill, E.T. (2019). A model of chronic, transmissible Otitis Media in mice. PLoS Pathog. *15*, e1007696.

Durack, J., Lynch, S.V., Nariya, S., Bhakta, N.R., Beigelman, A., Castro, M., Dyer, A.M., Israel, E., Kraft, M., Martin, R.J., et al. (2017). Features of the bronchial bacterial microbiome associated with atopy, asthma, and responsiveness to inhaled corticosteroid treatment. J. Allergy Clin. Immunol. *140*, 63–75.

Durinck, S., Spellman, P.T., Birney, E., and Huber, W. (2009). Mapping identifiers for the integration of genomic datasets with the R/Bioconductor package biomaRt. Nat. Protoc. *4*, 1184–1191.

Ehlers, A., Xie, W., Agapov, E., Brown, S., Steinberg, D., Tidwell, R., Sajol, G., Schutz, R., Weaver, R., Yu, H., et al. (2018). BMAL1 links the circadian clock to viral airway pathology and asthma phenotypes. Mucosal Immunol. *11*, 97–111.

Forteza, R.M., Ahmed, A., Lee, T., and Abraham, W.M. (2001). Secretory leukocyte protease inhibitor, but not alpha-1 protease inhibitor, blocks tryptase-induced bronchoconstriction. Pulm. Pharmacol. Ther. *14*, 107–110.

Ge, X.N., Ha, S.G., Greenberg, Y.G., Rao, A., Bastan, I., Blidner, A.G., Rao, S.P., Rabinovich, G.A., and Sriramarao, P. (2016). Regulation of eosinophilia and allergic airway inflammation by the glycan-binding protein galectin-1. Proc. Natl. Acad. Sci. USA *113*, E4837–E4846.

Goleva, E., Jackson, L.P., Harris, J.K., Robertson, C.E., Sutherland, E.R., Hall, C.F., Good, J.T., Jr., Gelfand, E.W., Martin, R.J., and Leung, D.Y. (2013). The effects of airway microbiome on corticosteroid responsiveness in asthma. Am. J. Respir. Crit. Care Med. *188*, 1193–1201.

Hayashimoto, N., Morita, H., Yasuda, M., Ishida, T., Kameda, S., Takakura, A., and Itoh, T. (2012). Prevalence of Bordetella hinzii in mice in experimental facilities in Japan. Res. Vet. Sci. *93*, 624–626.

Hiemstra, P.S., Maassen, R.J., Stolk, J., Heinzel-Wieland, R., Steffens, G.J., and Dijkman, J.H. (1996). Antibacterial activity of antileukoprotease. Infect. Immun. *64*, 4520–4524.

Hirota, K., Yoshitomi, H., Hashimoto, M., Maeda, S., Teradaira, S., Sugimoto, N., Yamaguchi, T., Nomura, T., Ito, H., Nakamura, T., et al. (2007). Preferential recruitment of CCR6-expressing Th17 cells to inflamed joints via CCL20 in rheumatoid arthritis and its animal model. J. Exp. Med. *204*, 2803–2812.

Hunt, S.E., McLaren, W., Gil, L., Thormann, A., Schuilenburg, H., Sheppard, D., Parton, A., Armean, I.M., Trevanion, S.J., Flicek, P., and Cunningham, F. (2018). Ensembl variation resources. Database (Oxford) *2018*, bay119.

Ivanov, Y.V., Linz, B., Register, K.B., Newman, J.D., Taylor, D.L., Boschert, K.R., Le Guyon, S., Wilson, E.F., Brinkac, L.M., Sanka, R., et al. (2016). Identification and taxonomic characterization of Bordetella pseudohinzii sp. nov. isolated from laboratory-raised mice. Int. J. Syst. Evol. Microbiol. *66*, 5452–5459.

Kanehisa, M., and Goto, S. (2000). KEGG: kyoto encyclopedia of genes and genomes. Nucleic Acids Res. *28*, 27–30.

Kau, A.L., Planer, J.D., Liu, J., Rao, S., Yatsunenko, T., Trehan, I., Manary, M.J., Liu, T.-C., Stappenbeck, T.S., Maleta, K.M., et al. (2015). Functional characterization of IgA-targeted bacterial taxa from undernourished Malawian children that produce diet-dependent enteropathy. Sci. Transl. Med. *7*, 276ra224.

Klaßen, C., Karabinskaya, A., Dejager, L., Vettorazzi, S., Van Moorleghem, J., Lühder, F., Meijsing, S.H., Tuckermann, J.P., Bohnenberger, H., Libert, C., and Reichardt, H.M. (2017). Airway Epithelial Cells Are Crucial Targets of Glucocorticoids in a Mouse Model of Allergic Asthma. J. Immunol. *199*, 48–61.

Kuperman, D.A., Lewis, C.C., Woodruff, P.G., Rodriguez, M.W., Yang, Y.H., Dolganov, G.M., Fahy, J.V., and Erle, D.J. (2005). Dissecting asthma using focused transgenic modeling and functional genomics. J. Allergy Clin. Immunol. *116*, 305–311.

Langmead, B., and Salzberg, S.L. (2012). Fast gapped-read alignment with Bowtie 2. Nat. Methods *9*, 357–359.

Liaw, A., and Wiener, M. (2002). Classification and Regression by randomForest. R News *2*, 18–22.

Livak, K.J., and Schmittgen, T.D. (2001). Analysis of relative gene expression data using real-time quantitative PCR and the 2(-Delta Delta C(T)) Method. Methods. *25*, 402–408.

Löhning, M., Stroehmann, A., Coyle, A.J., Grogan, J.L., Lin, S., Gutierrez-Ramos, J.C., Levinson, D., Radbruch, A., and Kamradt, T. (1998). T1/ST2 is preferentially expressed on murine Th2 cells, independent of interleukin 4, interleukin 5, and interleukin 10, and important for Th2 effector function. Proc. Natl. Acad. Sci. USA *95*, 6930–6935.

Loong, S.K., Che-Mat-Seri, N.A., Abdulrazak, O., Douadi, B., Ahmad-Nasrah, S.N., Johari, J., Mohd-Zain, S.N., and Abubakar, S. (2018). Recovery of Bordetella bronchiseptica sequence type 82 and B. pseudohinzii from urban rats in Terengganu, Malaysia. J. Vet. Med. Sci. *80*, 77–84.

Love, M.I., Huber, W., and Anders, S. (2014). Moderated estimation of fold change and dispersion for RNA-seq data with DESeq2. Genome Biol. *15*, 550.

Luo, W., Friedman, M.S., Shedden, K., Hankenson, K.D., and Woolf, P.J. (2009). GAGE: generally applicable gene set enrichment for pathway analysis. BMC Bioinformatics *10*, 161.

Mach, N., Gillessen, S., Wilson, S.B., Sheehan, C., Mihm, M., and Dranoff, G. (2000). Differences in dendritic cells stimulated in vivo by tumors engineered to secrete granulocyte-macrophage colony-stimulating factor or Flt3-ligand. Cancer Res. *60*, 3239–3246.

Marin, N.D., Dunlap, M.D., Kaushal, D., and Khader, S.A. (2019). Friend or Foe: The Protective and Pathological Roles of Inducible Bronchus-Associated Lymphoid Tissue in Pulmonary Diseases. J. Immunol. *202*, 2519–2526.

Marino, R., Thuraisingam, T., Camateros, P., Kanagaratham, C., Xu, Y.Z., Henri, J., Yang, J., He, G., Ding, A., and Radzioch, D. (2011). Secretory leukocyte protease inhibitor plays an important role in the regulation of allergic asthma in mice. J. Immunol. *186*, 4433–4442.

Matsuba, S., Yabe-Wada, T., Takeda, K., Sato, T., Suyama, M., Takai, T., Kikuchi, T., Nukiwa, T., and Nakamura, A. (2017). Identification of Secretory Leukoprotease Inhibitor As an Endogenous Negative Regulator in Allergic Effector Cells. Front. Immunol. *8*, 1538.

McCann, J.R., Mason, S.N., Auten, R.L., St Geme, J.W., 3rd, and Seed, P.C. (2016). Early-Life Intranasal Colonization with Nontypeable Haemophilus influenzae Exacerbates Juvenile Airway Disease in Mice. Infect. Immun. *84*, 2022–2030.

McGovern, T.K., Robichaud, A., Fereydoonzad, L., Schuessler, T.F., and Martin, J.G. (2013). Evaluation of respiratory system mechanics in mice using the forced oscillation technique. J. Vis. Exp., e50172.

McKinley, L., Alcorn, J.F., Peterson, A., Dupont, R.B., Kapadia, S., Logar, A., Henry, A., Irvin, C.G., Piganelli, J.D., Ray, A., and Kolls, J.K. (2008). TH17 cells mediate steroid-resistant airway inflammation and airway hyperresponsiveness in mice. J. Immunol. *181*, 4089–4097.

McMurdie, P.J., and Holmes, S. (2013). phyloseq: an R package for reproducible interactive analysis and graphics of microbiome census data. PLoS One *8*, e61217.

Nathan, R.A., Sorkness, C.A., Kosinski, M., Schatz, M., Li, J.T., Marcus, P., Murray, J.J., and Pendergraft, T.B. (2004). Development of the asthma control test: a survey for assessing asthma control. J. Allergy Clin. Immunol. *113*, 59–65.

National Asthma Education and Prevention Program (2007). Expert Panel Report 3 (EPR-3): Guidelines for the Diagnosis and Management of Asthma-Summary Report 2007. J. Allergy Clin. Immunol. *120*, S94–S138.

Newcomb, D.C., Boswell, M.G., Reiss, S., Zhou, W., Goleniewska, K., Toki, S., Harintho, M.T., Lukacs, N.W., Kolls, J.K., and Peebles, R.S., Jr. (2013). IL-17A inhibits airway reactivity induced by respiratory syncytial virus infection during allergic airway inflammation. Thorax *68*, 717–723.

Östling, J., van Geest, M., Schofield, J.P.R., Jevnikar, Z., Wilson, S., Ward, J., Lutter, R., Shaw, D.E., Bakke, P.S., Caruso, M., et al. (2019). IL-17-high asthma with features of a psoriasis immunophenotype. J. Allergy Clin. Immunol. *144*, 1198–1213.

Parameswaran, G.I., Sethi, S., and Murphy, T.F. (2011). Effects of bacterial infection on airway antimicrobial peptides and proteins in COPD. Chest *140*, 611–617.

Patnode, M.L., Bando, J.K., Krummel, M.F., Locksley, R.M., and Rosen, S.D. (2014). Leukotriene B4 amplifies eosinophil accumulation in response to nematodes. J. Exp. Med. *211*, 1281–1288.

Perniss, A., Schmidt, N., Gurtner, C., Dietert, K., Schwengers, O., Weigel, M., Hempe, J., Ewers, C., Pfeil, U., Gärtner, U., et al. (2018). Bordetella pseudohinzii targets cilia and impairs tracheal cilia-driven transport in naturally acquired infection in mice. Sci. Rep. *8*, 5681.

Persson, L.J., Aanerud, M., Hardie, J.A., Miodini Nilsen, R., Bakke, P.S., Eagan, T.M., and Hiemstra, P.S. (2017). Antimicrobial peptide levels are linked to airway inflammation, bacterial colonisation and exacerbations in chronic obstructive pulmonary disease. Eur. Respir. J. *49*, 1601328.

Preston, J.A., Essilfie, A.T., Horvat, J.C., Wade, M.A., Beagley, K.W., Gibson, P.G., Foster, P.S., and Hansbro, P.M. (2007). Inhibition of allergic airways disease by immunomodulatory therapy with whole killed Streptococcus pneumoniae. Vaccine *25*, 8154–8162.

Preston, J.A., Thorburn, A.N., Starkey, M.R., Beckett, E.L., Horvat, J.C., Wade, M.A., O'Sullivan, B.J., Thomas, R., Beagley, K.W., Gibson, P.G., et al. (2011). Streptococcus pneumoniae infection suppresses allergic airways disease by inducing regulatory T-cells. Eur. Respir. J. *37*, 53–64.

Puchta, A., Verschoor, C.P., Thurn, T., and Bowdish, D.M. (2014). Characterization of inflammatory responses during intranasal colonization with Streptococcus pneumoniae. J. Vis. Exp., e50490.

R Development Core Team (2011). R: A language and environment for statistical computing (R Foundation for Statistical Computing).

Raundhal, M., Morse, C., Khare, A., Oriss, T.B., Milosevic, J., Trudeau, J., Huff, R., Pilewski, J., Holguin, F., Kolls, J., et al. (2015). High IFN-γ and low SLPI mark severe asthma in mice and humans. J. Clin. Invest. *125*, 3037–3050.

Reddel, H.K., Bateman, E.D., Becker, A., Boulet, L.P., Cruz, A.A., Drazen, J.M., Haahtela, T., Hurd, S.S., Inoue, H., de Jongste, J.C., et al. (2015). A summary of the new GINA strategy: a roadmap to asthma control. Eur. Respir. J. *46*, 622–639.

Ridaura, V.K., Faith, J.J., Rey, F.E., Cheng, J., Duncan, A.E., Kau, A.L., Griffin, N.W., Lombard, V., Henrissat, B., Bain, J.R., et al. (2013). Gut microbiota from twins discordant for obesity modulate metabolism in mice. Science *341*, 1241214.

Rosshart, S.P., Herz, J., Vassallo, B.G., Hunter, A., Wall, M.K., Badger, J.H., McCulloch, J.A., Anastasakis, D.G., Sarshad, A.A., Leonardi, I., et al. (2019). Laboratory mice born to wild mice have natural microbiota and model human immune responses. Science *365*, eaaw4361.

Rosshart, S.P., Vassallo, B.G., Angeletti, D., Hutchinson, D.S., Morgan, A.P., Takeda, K., Hickman, H.D., McCulloch, J.A., Badger, J.H., Ajami, N.J., et al. (2017). Wild Mouse Gut Microbiota Promotes Host Fitness and Improves Disease Resistance. Cell *171*, 1015–1028.e1013.

Rudnicki, W.R., and Kursa, M.B. (2009). Feature Selection with the Boruta Package. J. Stat. Softw. *36*, 1–13.

Sallenave, J.M., Shulmann, J., Crossley, J., Jordana, M., and Gauldie, J. (1994). Regulation of secretory leukocyte proteinase inhibitor (SLPI) and elastase-specific inhibitor (ESI/elafin) in human airway epithelial cells by cytokines and neutrophilic enzymes. Am. J. Respir. Cell Mol. Biol. *11*, 733–741.

Schmitz, J., Owyang, A., Oldham, E., Song, Y., Murphy, E., McClanahan, T.K., Zurawski, G., Moshrefi, M., Qin, J., Li, X., et al. (2005). IL-33, an interleukin-1-like cytokine that signals via the IL-1 receptor-related protein ST2 and induces T helper type 2-associated cytokines. Immunity *23*, 479–490.

Schnyder-Candrian, S., Togbe, D., Couillin, I., Mercier, I., Brombacher, F., Quesniaux, V., Fossiez, F., Ryffel, B., and Schnyder, B. (2006). Interleukin-17 is a negative regulator of established allergic asthma. J. Exp. Med. *203*, 2715–2725.

Sergushichev, A.A. (2016). An algorithm for fast preranked gene set enrichment analysis using cumulative statistic calculation. bioRxiv. https://doi.org/10.1101/060012.

Shilts, M.H., Rosas-Salazar, C., Turi, K.N., Rajan, D., Rajagopala, S.V., Patterson, M.F., Gebretsadik, T., Anderson, L.J., Peebles, R.S., Jr., Hartert, T.V., and Das, S.R. (2020). Nasopharyngeal Haemophilus and local immune response during infant respiratory syncytial virus infection. J. Allergy Clin. Immunol., S0091-6749(20)30952-0.

Simpson, J.L., Daly, J., Baines, K.J., Yang, I.A., Upham, J.W., Reynolds, P.N., Hodge, S., James, A.L., Hugenholtz, P., Willner, D., and Gibson, P.G. (2016). Airway dysbiosis: Haemophilus influenzae and Tropheryma in poorly controlled asthma. Eur. Respir. J. *47*, 792–800.

Taggart, C.C., Cryan, S.A., Weldon, S., Gibbons, A., Greene, C.M., Kelly, E., Low, T.B., O'neill, S.J., and McElvaney, N.G. (2005). Secretory leucoprotease inhibitor binds to NF-kappaB binding sites in monocytes and inhibits p65 binding. J. Exp. Med. *202*, 1659–1668.

Thijs, W., Janssen, K., van Schadewijk, A.M., Papapoulos, S.E., le Cessie, S., Middeldorp, S., Melissant, C.F., Rabe, K.F., and Hiemstra, P.S. (2015). Nasal Levels of Antimicrobial Peptides in Allergic Asthma Patients and Healthy Controls: Differences and Effect of a Short 1,25(OH)2 Vitamin D3 Treatment. PLoS One *10*, e0140986.

Unhanand, M., Maciver, I., Ramilo, O., Arencibia-Mireles, O., Argyle, J.C., McCracken, G.H., Jr., and Hansen, E.J. (1992). Pulmonary clearance of Moraxella catarrhalis in an animal model. J. Infect. Dis. *165*, 644–650.

Wakashin, H., Hirose, K., Maezawa, Y., Kagami, S., Suto, A., Watanabe, N., Saito, Y., Hatano, M., Tokuhisa, T., Iwakura, Y., et al. (2008). IL-23 and Th17 cells enhance Th2-cell-mediated eosinophilic airway inflammation in mice. Am. J. Respir. Crit. Care Med. *178*, 1023–1032.

Wang, Q., Garrity, G.M., Tiedje, J.M., and Cole, J.R. (2007). Naive Bayesian classifier for rapid assignment of rRNA sequences into the new bacterial taxonomy. Appl. Environ. Microbiol. *73*, 5261–5267.

Whitehead, G.S., Thomas, S.Y., and Cook, D.N. (2014). Modulation of distinct asthmatic phenotypes in mice by dose-dependent inhalation of microbial products. Environ. Health Perspect. *122*, 34–42.

Wiedow, O., Harder, J., Bartels, J., Streit, V., and Christophers, E. (1998). Antileukoprotease in human skin: an antibiotic peptide constitutively produced by keratinocytes. Biochem. Biophys. Res. Commun. *248*, 904–909.

Wright, C.D., Havill, A.M., Middleton, S.C., Kashem, M.A., Lee, P.A., Dripps, D.J., O'Riordan, T.G., Bevilacqua, M.P., and Abraham, W.M. (1999). Secretory leukocyte protease inhibitor prevents allergen-induced pulmonary responses in animal models of asthma. J. Pharmacol. Exp. Ther. *289*, 1007–1014.

Zuberi, R.I., Apgar, J.R., Chen, S.S., and Liu, F.T. (2000). Role for IgE in airway secretions: IgE immune complexes are more potent inducers than antigen alone of airway inflammation in a murine model. J. Immunol. *164*, 2667–2673.

STAR★METHODS

KEY RESOURCES TABLE

REAGENT or RESOURCE	SOURCE	IDENTIFIER
Antibodies		
FITC anti-mouse CD4 (Clone GK1.5)	Biolegend	Cat# 100406; RRID: AB_312691
FITC anti-mouse CD11c (Clone N418)	Biolegend	Cat# 117306; RRID: AB_313775
PE anti-mouse CD44 (Clone IM7)	BD Pharmigen™	Cat# 553134; RRID: AB_394649
PE anti-mouse SiglecF (Clone E50-2240)	BD Pharmigen™	Cat# 562068; RRID: AB_10896143
PE anti-mouse IL-17A (Clone TC11-18H0.1)	Biolegend	Cat# 506904; RRID: AB_315464
PerCP-Cy™5.5 anti-mouse TCR β chain (Clone H57-597)	BD Pharmigen™	Cat# 560657; RRID: AB_1727575
PerCP anti-mouse CD45 (Clone 30-F11)	Biolegend	Cat# 103129; RRID: AB_893343
PE/Cyanine7 anti-mouse IFNγ (Clone XMG1.2)	Biolegend	Cat# 505825; RRID: AB_1595591
PE-Cy™7 anti-mouse CD11b (Clone M1/70)	BD Pharmigen™	Cat# 552850; RRID: AB_394491
PE/Cyanine7 anti-mouse CD62L (Clone MEL-14)	Biolegend	Cat# 104418; RRID: AB_313103
APC anti-mouse Ly6G (Clone 1A8)	Biolegend	Cat# 127613; RRID: AB_1877163
APC anti-mouse CD4 (Clone RM4-5)	Biolegend	Cat# 100516; RRID: AB_312719
APC anti-mouse TNFα (Clone MP6-XT22)	BD Pharmigen™	Cat# 561062; RRID: AB_2034022
APC anti-mouse TCR β chain (Clone H57-597)	Biolegend	Cat# 109212; RRID: AB_313435
APC anti-mouse CD45 (Clone 30-F11)	Biolegend	Cat# 103112; RRID: AB_312977
APC/Cyanine7 anti-mouse TCR β chain (Clone H57-597)	Biolegend	Cat# 109220; RRID: AB_893624
APC/Cyanine7 anti-mouse CD25 (Clone PC6)	Biolegend	Cat# 102026; RRID: AB_830745
APC/Cyanine7 anti-mouse I-A/I-E (Clone M5/114.15.2)	Biolegend	Cat# 107627; RRID: AB_1659252
eFluor450 anti-mouse FoxP3 (Clone FJK-16 s)	Thermo Fisher Scientific (eBioscience™)	Cat# 48-5773-82; RRID: AB_1518812
eFluor450 anti-mouse IL-13 (Clone 13A)	Thermo Fisher Scientific (eBioscience™)	Cat# 48-7133-80; RRID: AB_11219690
Brilliant Violet 421™ anti-mouse F4/80 (Clone BM8)	Biolegend	Cat# 123131; RRID: AB_10901171
APC/Cyanine7 anti-mouse/human CD45R/B220 (Clone RA3-6B2)	Biolegend	Cat# 103224; RRID: AB_313007
Brilliant Violet 421™ anti-mouse CD45.1 (Clone A20)	Biolegend	Cat# 110731; RRID: AB_10896425
PE anti-mouse TCR Vα2 (Clone B20.1)	Biolegend	Cat# 127807; RRID: AB_1134184
PerCP/Cyanine5.5 anti-mouse TCR Vα2 (Clone B20.1)	Biolegend	Cat# 127813; RRID: AB_1186118
APC anti-mouse TCR Vβ5.1, 5.2 (Clone MR9-4)	Biolegend	Cat# 139505; RRID: AB_10897800
PE/Cyanine7 anti-mouse TCR Vβ5.1, 5.2 (Clone MR9-4)	Biolegend	Cat# 139507; RRID: AB_2566020
PE anti-mouse IL-4 (Clone 11B11)	Thermo Fisher Scientific (eBioscience™)	Cat# 12-7041-82; RRID: AB_466156
Biotin anti-mouse CD11c (Clone N418)	Biolegend	Cat# 117304; RRID: AB_313773
Biotin anti-mouse CD4 (Clone RM4-4)	Biolegend	Cat# 116010; RRID: AB_2561504

(*Continued on next page*)

Continued

REAGENT or RESOURCE	SOURCE	IDENTIFIER
Rat anti-mouse CD16/CD32 (Clone 2.4G2)	BD Bioscience	Cat# 553141; RRID: AB_394656
LEAF TM Purified anti-mouse I-A/I-E (Clone M5/114.15.2)	Bioegend	Cat# 107610; RRID: AB_2813968
Mouse anti-Ovalbumin antibody (Clone 2C6)	Bio-Rad	Cat# MCA2259; RRID: AB_2285753
Rat Anti-Mouse IgE-HRP (Clone 23G3)	SouthernBiotech	Cat# 1130-05; RRID: AB_2794618
*InVivo*mAb anti-mouse IL-17A(Clone 17F3)	BioXcell	Cat# BE0173; RRID: AB_10950102
*InVivo*mAb mouse IgG1 isotype control, unknown specificity(Clone MOPC21)	BioXcell	Cat# BE0083; RRID: AB_1107784
BUV737 Anti-mouse CD19 (Clone 1D3)	BD Biosciences	Cat# 612782; RRID: AB_2870111
BUV395 Anti-mouse CD45 (Clone 30-F11)	BD Biosciences	Cat# 565967; RRID: AB_2739420
BV750 Anti-mouse CD69 (Clone H1.2F3)	BD Biosciences	Cat# 747481; RRID: AB_2872156
Pacific Blue™ Anti-mouse/human CD44 (IM7)	Biolegend	Cat# 103019; RRID: AB_493682
Super Bright 436 Anti-mouse CD80 (Clone 16-10A1)	Thermo Fisher Scientific (eBioscience™)	Cat# 62-0801-80; RRID: AB_2716995
Brilliant Violet 421™ Anti-mouse CD196 (CCR6) (Clone 29-2L17)	Biolegend	Cat# 129817; RRID: AB_10898320
BD Horizon™ BV480 Anti-mouse CD103 (Clone M290)	BD Biosciences	Cat# 566201; RRID: AB_2739592
Brilliant Violet 510™ Anti-mouse CD183 (CXCR3) (Clone CXCR3-173)	Biolegend	Cat# 126527; RRID: AB_2562204
Brilliant Violet 570™ Anti-mouse Ly6G (Clone 1A8)	Biolegend	Cat# 127629; RRID: AB_10899738
Brilliant Violet 605™ Anti-mouse CD8a (Clone 53-6.7)	Biolegend	Cat# 100743; RRID: AB_2561352
Brilliant Violet 650™ Anti-mouse CD11b (Clone M1/70)	Biolegend	Cat# 101239; RRID: AB_11125575
Brilliant Violet 711™ Anti-mouse I-A/I-E (MHCII) (Clone M5/114 15.2)	Biolegend	Cat# 107643; RRID: AB_2565976
Brilliant Violet 785™ Anti-mouse CD11c (Clone N418)	Biolegend	Cat# 117335; RRID: AB_11219204
Alexa Fluor 532 Anti-mouse CD4 (Clone RM4-5)	Thermo Fisher Scientific (eBioscience™)	Cat# 58-0042-82; RRID: AB_11218891
PerCP-eFluor710 Anti-mouse CD64 (Clone X54-5/7.1)	Thermo Fisher Scientific (eBioscience™)	Cat# 46-0641-80; RRID: AB_2735015
FITC Anti-mouse IgE (Clone RME-1)	Biolegend	Cat# 406905; RRID: AB_493288
FITC Anti-mouse FcεRIα (Clone MAR-1)	Biolegend	Cat# 134305; RRID: AB_1626102
PerCP/Cyanine5.5 Anti-mouse CD193 (CCR3) (Clone J073E5)	Biolegend	Cat# 144515; RRID: AB_2565741
PE/Dazzle™ 594 Anti-mouse CD25 (Clone PC61)	Biolegend	Cat# 102047; RRID: AB_2564123
PE/Cyanine5 Anti-mouse CD117 (ckit) (Clone 2B8)	Biolegend	Cat# 105809; RRID: AB_313218
APC/Fire™ 750 anti-mouse TCR β chain (Clone H57-597)	Biolegend	Cat# 109245; RRID: AB_2629696
Alexa Fluor 700 Anti-mouse NK 1.1 (Clone PK136)	Biolegend	Cat# 108729; RRID: AB_2074426
APC Anti-mouse CD194 (CCR4) (Clone 2G12)	Biolegend	Cat# 131211; RRID: AB_1279135
Anti-mouse IL-33Rα (St2) Biotin (Clone DIH9)	Biolegend	Cat# 145307; RRID: AB_2565735

(*Continued on next page*)

Continued

REAGENT or RESOURCE	SOURCE	IDENTIFIER
Anti-mouse CD11c (Clone N418)	STEMCELL Technologies (Easysep)	Cat# 60002BT.1
Bacterial and Virus Strains		
Bordetella pseudohinzii strain 2-1 and 5-5	Isolated from two different male C57BL/6J mice bred in house	NA
Streptococcus, *Moraxella* and *Haemophilus*	Isolated from nasal lavage fluid of asthmatic and non-asthmatic individuals. Nasal lavage fluid were plated onto *Streptococcus* selective agar (BBL), *M. catarrhalis* selective agar (Remel), and *Haemophilus* selective agar (Remel).	NA
Escherichia coli (DH5α)	ATCC	Cat# 98489
Biological Samples		
Nasal and oral lavages were obtained from both an adult (ages 18-40 years) and a pediatric population (ages 6-10 years).	The study cohorts came from the Microbiota in Asthma Research Study (MARS	NA
Chemicals, Peptides, and Recombinant Proteins		
RPMI-1640 Medium	Milipore Sigma (Sigma Aldrich)	Cat# R8758
DMEM, low glucose, pyruvate	Thermo Fisher Scientific (GIBCO™)	Cat# 11885084
Trypsin	Thermo Fisher Scientific (GIBCO™)	Cat# 25300-54
Fetal Bovine Serum	Thermo Fisher Scientific (GIBCO™)	Cat# 26140-079
2-Mercaptoethanol	Milipore Sigma (Sigma Aldrich)	Cat# M3148
ACK Lysing Buffer	Thermo Fisher Scientific (GIBCO™)	Cat# A10492-01
HBSS, no calcium, no magnesium, no phenol red	Thermo Fisher Scientific (GIBCO™)	Cat# 14175079
Albumin from chicken egg white (Ovalbumin) - Grade V	Milipore Sigma (Sigma Aldrich)	Cat# A5503
Imject™ Alum Adjuvant	Thermo Scientific™	Cat# 77161
Acetyl-β-methylcholine chloride	Milipore Sigma (Sigma Aldrich)	Cat# A2251
DNase I	Milipore Sigma (Roche)	Cat# 10104159001
Liberase™ DL Research Grade	Milipore Sigma (Roche)	Cat# 5401160001
Defib sheep blood	HemoStat Laboratories	Cat# DSB050
BD Difco Brain Heart Infusion Agar	Fisher Scientific (BD)	Cat# DF0418-07-9
BD BBL Prepared Plated Media: Group A Selective Strep Agar with 5% Sheep Blood (ssA)	Fisher Scientific (BD)	Cat# L21779
Remel Catarrhalis Selective Medium	Thermo Fisher Scientific	Cat# R01575
Remel Haemophilus Isolation Agar w/ bacitracin and horse blood	Thermo Fisher Scientific	Cat# R01470
Phosphate Buffered Saline (PBS) 10X Powder	Fisher Scientific	Cat# BP665-1
Phenol/Chloroform/Isoamyl Alcohol	Fisher Chemical	Cat# BP1752I400
Triton™ X-100	Milipore Sigma (Sigma Aldrich)	Cat# T8787
TRIzol™ Reagent	Thermo Fisher Scientific (Invitrogen™)	Cat# 15596018
32% Paraformaldehyde	Fisher Scientific (Electron Microscopy Sciences)	Cat# 50-980-494
Penicillin-Streptomycin	Milipore Sigma (Roche)	Cat# 11074440001
Phorbol 12-myristate 13-acetate (PMA)	Milipore Sigma (Sigma Aldrich)	Cat# P8139
Ionomycin from *Streptomyces conglobatus*	Milipore Sigma (Sigma Aldrich)	Cat# I9657
Brefeldin A	Thermo Fisher Scientific	Cat# 00-4506-51
Monensin	Thermo Fisher Scientific	Cat# 00-4505-51
PowerSYBR Green PCR Master Mix	Thermo Fisher Scientific	Cat# 4367659

(*Continued on next page*)

Continued

REAGENT or RESOURCE	SOURCE	IDENTIFIER
Recombinant Human IL-1β	Biolegend	Cat# 579402
Recombinant Human TNFα	Biolegend	Cat# 570102
Recombinant Human IL-17A	Biolegend	Cat# 570502
Streptavidin BUV563	BD Biosciences	Cat# 612935
Critical Commercial Assays		
ELISA MAX Standard Set Mouse IL-17A	Biolegend	Cat# 432501
ELISA MAX Standard Set Mouse IL-4	Biolegend	Cat# 431101
RNAeasy Mini kit	QIAgen	Cat# 74104
Qubit™ Protein Assay Kit	Thermo Fisher Scientific	Cat# Q33211
NEBNext® Ultra II Directional RNA Library Prep Kit for Illumina®	New England Biolabs	Cat# E7760S
Mouse SLPI DuoSet ELISA	R&D Systems	Cat# DY1735-05
EasySep Mouse CD4 Positive Selection Kit II	STEMCELL technologies (Easysep)	Cat# 18952
EasySep Mouse CD11c Positive Selection Kit II with Spleen Dissociation Medium	STEMCELL Technologies (Easysep)	Cat# 18781
Human SLPI DuoSet ELISA	R&D Systems	Cat# DY1274-05
Quant-it Ribogreen RNA assay kit	Invitrogen™	Cat# R11490
High-Capacity cDNA Reverse Transcription Kit	Thermo Fisher Scientific	Cat# 4368814
NucleoSpin RNA XS, Micro kit	Macherey-Nagel	Cat# 740902.50
CellTrace CFSE Cell Proliferation Kit	Thermo Fisher Scientific (Invitrogen™)	Cat# C34554
LIVE/DEAD Fixable Aqua Dead Cell Stain Kit, for 405 nm excitation	Thermo Fisher Scientific (Invitrogen™)	Cat# L34966
NucleoSpin RNA XS	Machery-Nagel	Cat# 740902.50
Deposited Data		
Sequencing data	This paper	European Nucleotide Archive, PRJEB36780
Experimental Models: Cell Lines		
A549 (Human alveolar epithelial adenocarcinoma)	ATCC	Cat# CCL-185
B16-FLT3L expressing melanoma cells	Mach et al., 2000	NA
Experimental Models: Organisms/Strains		
Mouse: WT C57BL/6J: C57BL/6J	The Jackson Laboratory (Bar Harbor, ME)	Cat# 000664
Mouse: RAG1$^{-/-}$ C57BL/6J: B6.129S7-Rag1^{tm1Mom}/J	The Jackson Laboratory (Bar Harbor, ME)	Cat# 002216
Mouse: OTII: OTII Rag1$^{+/-}$ Ly5.1$^{+/-}$ Foxp3-GFP	bred in house	NA
Mouse: Germ-free C57BL/6J: WT C57BL/6J	bred in house	NA
Software and Algorithms		
R version 3.5.3 or higher	R Development Core Team, 2011	https://www.r-project.org/
FlowJo v10	BD	RRID: SCR_008520, https://www.flowjo.com/solutions/flowjo/downloads
GraphPad Prism 8	GraphPad software	RRID: SCR_002798, https://www.graphpad.com/scientific-software/prism/
BD FACSDiva™ software	BD Bioscience	RRID: SCR_001456
SPAdes version 3.11.0	Bankevich et al., 2012	https://cab.spbu.ru/software/spades/
BLAST version 2.6.0	Altschul et al., 1990.	https://blast.ncbi.nlm.nih.gov/Blast.cgi

(*Continued on next page*)

Continued

REAGENT or RESOURCE	SOURCE	IDENTIFIER
Ensembl, GRCm38.p6, release 98	Hunt et al., 2018	ftp://ftp.ensembl.org/pub/release-98/fasta/mus_musculus/dna/
bowtie2 version 2.3.4.1	Langmead and Salzberg, 2012	http://bowtie-bio.sourceforge.net/bowtie2/index.shtml
htseq version 0.9.1	Anders et al., 2015	https://htseq.readthedocs.io/en/master/
DESeq2 version 1.22.2	Love et al., 2014	https://bioconductor.org/packages/release/bioc/html/DESeq2.html
fgsea version 1.8	Sergushichev, 2016	https://bioconductor.org/packages/release/bioc/html/fgsea.html
gage version 2.32.1	Luo et. al 2009	https://www.bioconductor.org/packages/release/bioc/html/gage.html
Aperio ImageScope software	Leica Byosystems	RRID:SCR_014311
DADA2 (version 1.10.1 in R)	Callahan et al., 2016	https://benjjneb.github.io/dada2/
phyloseq (version 1.28.0) in R (version 3.6.1)	McMurdie and Holmes, 2013.	https://joey711.github.io/phyloseq/
randomForest v 4.6-14	Liaw and Wiener, 2002	NA
Boruta version 6.0.0	Rudnicki and Kursa, 2009	https://cran.r-project.org/web/packages/Boruta/index.html
biomaRt version 2.38.0, ensmebl archive Sept 2019	Durinck et al., 2009	https://bioconductor.org/packages/release/bioc/html/biomaRt.html

RESOURCE AVAILABILITY

Lead Contact

Further information and requests for resources and reagents should be directed to and will be fulfilled by the Lead Contact, Andrew Kau (akau@wustl.edu).

Materials Availability

All unique/stable reagents generated in this study are available from the Lead Contact with a completed Materials Transfer Agreement.

Data and Code Availability

The accession number for the sequencing data from RNA-seq, genome sequencing assemblies, and 16S rRNA sequencing reported in this paper is European Nucleotide Archive: PRJEB36780.

EXPERIMENTAL MODEL AND SUBJECT DETAILS

Human Subjects

The study cohorts came from the Microbiota in Asthma Research Study (MARS), which was designed to investigate the contribution of the human airway and gut microbiota to asthma. Both an adult (ages 18-40 years) and a pediatric population (ages 6-10 years) were recruited from the St. Louis, Missouri area. Inclusion criteria for the asthmatic cohort included: (1) A physician diagnosis of moderate-to-severe asthma. We also used a prescription of either a medium to high dose inhaled corticosteroid, or a combination of inhaled corticosteroid with either a leukotriene antagonist or long-acting beta-agonist as evidence of moderate to severe asthma (This corresponds to step 3 of the Expert Panel Report 3 guidelines (National Asthma Education and Prevention Program, 2007). (2) Evidence of allergic sensitization with at least one positive skin prick test to a panel of aeroallergens or by the presence of aeroallergen-specific serum IgE. (3) A recent prescription of a course of oral corticosteroids within two years of enrollment. The healthy cohort included individuals without a self-reported history of wheezing or shortness of breath within 1 year of recruitment or a history of asthma, allergic rhinitis, food allergy or eczema. Additionally, both asthmatic and healthy study participants were excluded if they received antibiotics within 30 days of their study visit, if they had major surgery on the sinuses, lung or gastrointestinal tract or if they had another serious medical condition other than asthma. All samples described in this study were obtained during the enrollment visit when asthmatic subjects were not experiencing an exacerbation, as defined by the need for oral corticosteroids. Written informed consent documents were obtained from all patients or their legal guardians, and the protocol was approved by the Washington University Institutional Review Board (IRB ID# 201412035).

Oral lavage samples were obtained by having each subject swish 20 mL of sterile saline in their mouth for 30 s before spitting into a sterile container for further processing. Nasal lavage specimens were collected as described (Allen et al., 2013). Briefly, 5 mL of sterile saline was instilled into each nostril while the participant has his/her head tilted backward. After 5 s, the patient tilted their head forward and the nasal lavage fluid was collected into a sterile cup. To minimize the saline running into the back of subjects' throats, we had patients repeat the sound "k-k-k" after administering saline. Separate oral and nasal lavage aliquots were either stored without additional processing (used for ELISA) or with a final concentration of 15% glycerol (for bacterial culture) and then stored at −80 C.

As summarized in Table S3, a total of 93 participants were included in this analysis. Steroid dose was categorized based on previously published studies (Reddel et al., 2015). All available samples were used for each analysis.

Experimental Animals and Ethics

Animal experiments were reviewed by the Washington University Institutional Animal Care and Use Committee (Protocol #20180286). Male wild-type (WT) and RAG1$^{-/-}$ C57BL/6J mice were obtained from Jackson Laboratory (Bar Harbor, ME); OTII Rag1$^{+/-}$ Ly5.1$^{+/-}$ Foxp3-GFP and germ-free mice were bred in house for these experiments. Mice were maintained under either specific pathogen free (SPF) conditions or in a BSL-2 facility when colonized with *B. pseudohinzii*. Germ-free mice were maintained in a gnotobiotic facility using flexible plastic isolators and monitored monthly to ensure sterility. All animals were housed 5 animals per cage maximum and their welfare assessed daily after colonization. All mice were between 6 and 8 weeks old.

Bacterial Strains and Growth Conditions

Bordetella pseudohinzii strain 2-1 and 5-5 were isolated on Brain heart infusion (BHI) agar supplemented with 5% sheep's blood from the bronchoalveolar lavage (BAL) of two different male C57BL/6J mice. We initially established that this strain was closely related to *Bordetella hinzii* by using selective PCR primers (Hayashimoto et al., 2012) and then conclusively identified this strain as *Bph* by whole genome sequencing (see below). For colonizations, *Bph* was grown overnight in BHI broth with shaking at 37°C. *Bph* strain 2-1 was used in all experiments unless otherwise noted. *E. coli* strain DH5a was grown in Luria Broth at 3C overnight with shaking.

Nasal lavage culture

We used a selective culture approach to quantify the amounts of live *Streptococcus*, *Moraxella* and *Haemophilus* present in nasal lavage fluid of asthmatic and non-asthmatic individuals. 100 μl of nasal lavage fluid from each participant were plated onto *Streptococcus* selective agar (BBL), *M. catarrhalis* selective agar (Remel), and *Haemophilus* selective agar (Remel). *M. catarrhalis* selective plates were incubated for 24 hours at 37°C, while *Haemophilus* and *Streptococcus* selective plates were grown for 24 h at 37°C in the presence of 5% CO2. We enumerated *Streptococcus* colonies that demonstrated alpha-hemolysis on *Streptococcus* selective plates; *Moraxella* as colonies that showed gamma-hemolysis on selective plates; and *Haemophilus* as colonies that were gamma-hemolytic on *Haemophilus* selective plates. The numbers of colonies were semiquantitatively assessed with the absence of growth as "0," presence of 1-50 c.f.u. as "1+," presence of 51-100 c.f.u. as "2+," presence of 101-300 c.f.u. as "3+" and > 300 c.f.u. as "4+." Contamination by other organisms was detected by 16S rRNA sequencing (see below) of plate sweeps of agar plates. If the presence of Moraxellaceae, Streptococcaceae, and Pasteurellaceae was not detected by 16S rRNA sequencing on their respective plate sweeps, growth was noted as "0."

METHOD DETAILS

Colonization with Bph

Bph cultures were resuspended in PBS then diluted to approximately 10^5 CFU/ml. To nasally colonize mice, we anesthetized mice with ketamine/xylazine then pipetted a total of 50 μl of *Bph* into the nares of sedated animals with the goal of delivering ~10^4 CFU to each mouse. For mice receiving HK *Bph*, we autoclaved (125°C for 20 minutes) an aliquot of PBS *Bph* suspension to deliver a dose of ~10^4 CFU of HK *Bph* and confirmed the absence of viable bacteria by culture.

Bph Genome Sequencing

DNA was isolated from overnight cultures of *Bph* using bead-beating with phenol-chloroform extraction. The extracted and purified DNA was then sheared to 150 bp using a Covaris E220 sonicator. Barcoded sequencing adapters were then ligated to A-tailed, end-repaired DNA fragments (Chen et al., 2013) which were then amplified and sequenced using a MiSeq (Illumina) with paired-end 250 bp reads. Genome sequences were then assembled using SPAdes (Bankevich et al., 2012). Virulence factors in Bordetella genomes were identified by BLAST (Altschul et al., 1990) against a database of genes from the Virulence Factor Database (Chen et al., 2016).

Enumeration of Bph

BAL (Patnode et al., 2014) and nasal lavage were obtained as described (Puchta et al., 2014). Lungs were perfused with sterile PBS before being removed and 2 mm of tracheas were excised before homogenizing each tissue in 1 mL of PBS with 0.025% Triton X-100. Samples were then serially diluted then spotted onto BHI Blood Agar plates and colonies counted after 18h. Antibiotic markers were not available, so colony morphology was used to identify *Bph*. Additionally, we confirmed the presence of *Bph* in samples by V4

16S rRNA sequencing (see below). Typically, we observed no CFU from the BALs, lungs or tracheas of non-colonized animals. Nasal lavages from *Bph* colonized animals had ~10^3 more total CFU than non-colonized animals.

Asthma model

Allergic airway inflammation (AAI) was induced in mice using chicken egg ovalbumin (OVA), as previously described (Kuperman et al., 2005). Mice were sensitized on days 0, 7 and 14 by i.p. injections of OVA (50 μg, Sigma grade V) complexed with aluminum potassium sulfate (Imject Alum, Thermo Scientific) in a total volume of 200 μL in sterile PBS 1X. Mice were then challenged intranasally with OVA (1 mg in 50 μL of sterile PBS, or 20 mg/ml) on days 20-22 under anesthesia. Control mice were sensitized and challenged with PBS 1X unless otherwise noted. On day 23, mice were sacrificed and tissues were collected for further analysis.

Processing of mouse tissue for RNA and protein

We isolated total RNA from mouse tissue as previously described (Ridaura et al., 2013). Briefly, whole lungs were removed from mice and homogenized in 2 mL of Trizol reagent. Crude RNA was then extracted from a 0.3 mL portion of the homogenized tissue and then purified using the RNAeasy kit, according to the manufacturer's protocol (QIAgen). If protein quantification in addition to RNA profiling was planned, mouse lungs were flash-frozen in liquid nitrogen at the time of sacrifice, then pulverized while still frozen then aliquoted and stored at −80°C until used for RNA extraction (as above) or protein quantification. For protein ELISAs pulverized aliquots were homogenized in PBS supplemented with protease inhibitor cocktail followed by centrifugation at 16,000 *rcf.* for 20 minutes and the supernatant retained. Samples were normalized to total protein quantitated using Qubit protein assay kit (Fisher Q33211)

Transcriptional profiling of mouse lungs

RNA quality was then assessed using a BioAnalyzer (Agilent) to ensure that all samples had an RNA integrity number greater than 8.0. Stranded, poly-A enriched libraries were then generated using the NEBnext Ultra II library prep kit according to the kit's instructions and sequenced on two lanes of a HiSeq3000 using 1x50 bp chemistry. An average of 36,338,433 reads (with a standard deviation of 13.3 million reads) were obtained per sample. After demultiplexing these data, reads were mapped to the mouse genome downloaded from Ensembl (GRCm38.p6, release 98; Hunt et al., 2018) using bowtie2 (Langmead and Salzberg, 2012) and reads were quantified at the gene level using htseq (Anders et al., 2015). All technical replicates retained high similarity (Spearman rho > 0.93) and were combined for further analysis. Differentially expressed transcripts were identified using DESeq2 (Love et al., 2014). Transcripts were mapped to corresponding entrez ID using biomaRt (Durinck et al., 2009) and were used to identify genes (Figure 5B) and pathways of interest. Functional pathways altered during colonization and/or AAI were identified by gene set enrichment analysis using fgsea (Sergushichev, 2016) using the Kyoto Encyclopedia of Genes and Genomes database (Kanehisa and Goto, 2000) accessed through the gage R package (Luo et al., 2009).

Histopathology

Lung right lobe was collected in 4% PFA and tissue sections were prepared from paraffin block and stained with H&E. Whole lung was collected and stored in 4% PFA for 24 hours, then rinsed with 70% ethanol. Tissue sections were prepared from paraffin blocks and stained with PAS. Slides were analyzed on a Nanozoomer 2.0-HT at x20 and x40 objectives. The six largest airways were then analyzed using Aperio ImageScope software (Ge et al., 2016) positive pixel count algorithm. A ratio was calculated as the number of strong positive pixels (NSP) to the number of total pixels (Ntotal) (Ehlers et al., 2018).

16 s rRNA sequencing

DNA extracts were generated from fecal or cecal samples by phenol-chloroform extraction with bead beating as previously described (Kau et al., 2015). 16S amplicons were generated using indexed primers (Caporaso et al., 2011) and sequenced using a MiSeq with paired-end 250 bp reads. To process these data, we used DADA2 (version 1.10.1 in R) to generate amplicon sequence variants (ASVs) from the demultiplexed data (Callahan et al., 2016). Forward and reverse reads were merged, chimeras were removed, and taxonomy was assigned using the inbuilt DADA2 function for the RDP Classifier (Wang et al., 2007) with a custom database described in Kau et al. (2015) and minimum bootstrap support of 80%.

Analysis of 16S data was carried out using phyloseq (version 1.28.0) in R (version 3.6.1) (McMurdie and Holmes, 2013). Random forest was carried out using the randomForest (Liaw and Wiener, 2002) for feature selection as described in Rudnicki and Kursa (2009). Briefly, random forest was carried out in regression mode with SLPI levels measured by ELISA in oral lavage samples as the response and relative abundance of ASVs from 16S sequencing of oral lavage as predictors. Additionally, randomly permuted versions of each predictor, termed shadow variables, were included. After each iteration of Random Forest, the importance scores of the predictors were compared to the importance scores of their shadow variables. Predictors and their shadow variables were removed if the predictors were not more important than their shadows a significant number of times. After 100 iterations of Boruta, predictors that were selected more often than by chance alone were used in the final model.

Lymphocyte isolation from tissues

Mouse lung tissue was dissociated as previously reported (Patnode et al., 2014). Lungs were minced and incubated in digestion buffer (0.2 U/ml Liberase DL (Roche Applied Sciences) and 0.2 mg/ml DNase (Sigma) in Hank's Buffered Salt Solution (without

Ca^{2+}/Mg^{2+}) for 25 min at 37°C before being passed through a 70μm cell strainer. Spleen and lymph nodes were dissociated manually and passed through a 70μm cell strainer. Red blood cells were removed from lung and spleen samples by treating with ACK lysis buffer.

Restimulation assays

$CD4^+$ lymphocytes from the lung, spleen and lymph nodes were purified via antibody-conjugated magnetic bead separation with the anti-CD4 kit from STEMCELL technologies (Easysep). Antigen-presenting cells (APCs) were harvested from the spleen of mice that had been injected 7 days previously with $1x10^6$ B16-FLT3L expressing melanoma cells (Mach et al., 2000). APCs were isolated using the anti-CD11c kit from STEMCELL Technologies following the manufacture protocol. Bacterial antigens were prepared by resuspending bacteria from an overnight culture in PBS, autoclaving for 15 minutes, then normalizing to total protein content. $5x10^4$ $CD11c^+$ cells were incubated with 5 or 20 μg of *Bph* and *E. coli* antigen or 500 μg of OVA for 30 min. $1x10^5$ $CD4^+$ cells stained with Cell Trace FITC (Invitrogen™) were then added to the $CD11c^+$ cells and incubated for 72 hours at 37°C. For restimulation of splenocytes, $7.5x10^5$/ml cells were stained with Cell Trace FITC, then incubated with *Bph* proteins or OVA for 72 hours at 37°C. For MHC class II blocking experiments, $CD11c^+$ cells were treated with 20 μg/mL anti-MHC class II blocking antibody for 30 minutes before adding bacterial proteins. All cells were cultured in DMEM supplemented with 10% FBS, 100 U/ml penicillin, 100 mg/ml streptomycin and 100mM 2-mercaptoethanol.

FACS assays

For intracellular staining of cytokines, cells were stimulated for 4 h at 37°C with PMA (10ng/mL), ionomycin (200ng/mL), monensin (1:1000), and brefeldin A (1:1000). LIVE/DEAD Fixable Aqua Dead Cell Stain Kit was used to assess cell viability in all panels. Data were acquired on a FACS Canto II (BD Biosciences) equipped for the detection of eight fluorescent parameters or for Figures 4H and 4I, a five-laser Aurora (Cytek Biosciences). Data analysis was performed using FlowJo version 10 or higher software (Treestar, Ashland, OR).

Protein quantification by ELISA

IL-17A (Biolegend) and mouse SLPI (R&D Systems DY1735-05), and human SLPI (R&D Systems DY1274-05) ELISAs were performed according to the manufacturer's protocol. Mouse serum OVA-specific IgE was quantified by sandwich ELISA (Zuberi et al., 2000). Briefly, plates were coated with 10μg/mL of OVA overnight at 4°C and then blocked with PBS 1x + 0.1% BSA. Serum (1:25 dilution) was placed in the wells and incubated for 2 h at room temperature. OVA-specific monoclonal IgE (Bio-Rad Cat No. MCA2259. Clone 2C6) was used as the standard curve. The bound IgE was detected by Rat anti-mouse IgE-HRP (Southern Biotech Cat No. 1130-05. Clone 23G3).

Quantitative PCR

RNA quality was assessed by gel electrophoresis and quantitated using Quant-it Ribogreen RNA assay kit (Invitrogen R11490). cDNA was synthesized using High-Capacity cDNA Reverse Transcription Kit at 500 ng RNA input (Fisher 4368814). qPCR was then performed using primers described in Table S4 using PowerSYBR Green PCR Master Mix (Fisher 4367659). Results were analyzed using the ddCT method (Livak and Schmittgen, 2001).

Measurement of Airway Hyperresponsiveness

We assessed murine airway physiology using a Flexivent with FX1 attachment. Mice were anesthetized using 10 mg/ml ketamine, 1 mg/ml xylazine cocktail and the trachea surgically cannulated (McGovern et al., 2013). After i.p. Injection of neuromuscular blockade with pancuronium (0.8 mg/kg) (Whitehead et al., 2014), we administered escalating doses of nebulized methacholine (0, 1.56, 3.125, 6.25, 12.5, 25 mg/ml) and assessed measures of respiratory mechanics as described in the main text using area under the curve measurements for each methacholine dose.

IL-17A neutralization

C57BL/6J mice were i.p. injected with a loading dose (500μg/mouse) of neutralizing anti-IL-17A antibody (BioXcell 17F3 BE0173) or IgG isotype control (BioXcell MOPC21 BE0083). Subsequent does (100μg/mouse) were administered 3 times weekly as depicted in the experimental schematics.

Adoptive transfer of naive T $CD4^+$ cells

Lymphocytes from the spleen and lymph nodes of an OTII $Rag1^{+/-}$ $Ly5.1^{+/-}$ Foxp3-GFP mice were collected as described above. Naive ($CD4^+CD44^-CD62L^+$ $FoxP3^-$) cells were sorted into DMEM 10% using a FACS AriaII (BD Biosciences) and $5x10^4$ cells per mouse were injected i.v. on day 15 of AAI model.

A549 cell culture

Human alveolar epithelial adenocarcinoma (A549) were obtained from ATCC (CCL-185) and maintained in Dulbecco's Modified Eagles Medium (DMEM; GIBCOTM Cat. No. 31600-034) supplemented with 10% fetal bovine serum (FBS; GIBCO Cat. No. 16000-044)

and 0.1 mg/mL of penicillin–streptomycin antibiotic (GIBCO Cat. No.15140122). Cells were maintained at 37°C and 5% CO_2 in a humidified incubator with medium being replaced every 48 h.

To assess Slpi expression in response to cytokines, A549 cells ($5x10^4$) were plated on 24-well culture plates until they reached 50% confluence. Cells were starved (0.5% FBS) for 24 h then treated with IL-1β (1 ng/ml; Biolegend 579402), TNFα (10 ng/ml; Biolegend 570102), IL-17A (100 ng/ml; Biolegend 570502), TNFα plus IL-17A (10 ng/ml; 100 ng/ml) for 14 h at 37°C and 5% CO_2. The supernatants were collected and the cells were lysed and stored in Trizol at −80°C. RNA was isolated from A549 cells stored in Trizol using the Macherey-Nagel Nucleospin RNA XS Kit according to the manufacturer's protocol and qRT-PCR was performed as described above.

QUANTIFICATION AND STATISTICAL ANALYSIS

Statistical analysis was performed using Graphpad Prism 5.02 (GraphPad Software, La Jolla, CA) or R (R Development Core Team, 2011). Data are presented as the mean with error bars denoting SEM, box and whisker plots or scatterplots. Unless otherwise noted, statistically significant differences between groups with continuous data were determined by paired or unpaired Mann-Whitney U/Wilcoxon test, as indicated in the figures. For comparisons with multiple groups, we first performed a Kruskal-Wallace test and, if significant, performed a post hoc Wilcoxon with adjustment of p values for multiple hypotheses using BH correction. For categorical data, significance was determined using Fisher's exact test. Associations were determined using Spearman's Rank. In all figures, the following symbols were used to designate significance: n.s. = not significant, $p > 0.05$, * $p < 0.05$, ** $p < 0.01$, *** $p < 0.001$, **** $p < 0.0001$.

Cell Reports, Volume *33*

Supplemental Information

Airway Microbiota-Host Interactions Regulate Secretory Leukocyte Protease Inhibitor Levels and Influence Allergic Airway Inflammation

Natalia Jaeger, Ryan T. McDonough, Anne L. Rosen, Ariel Hernandez-Leyva, Naomi G. Wilson, Michael A. Lint, Emilie V. Russler-Germain, Jiani N. Chai, Leonard B. Bacharier, Chyi-Song Hsieh, and Andrew L. Kau

Figure S1

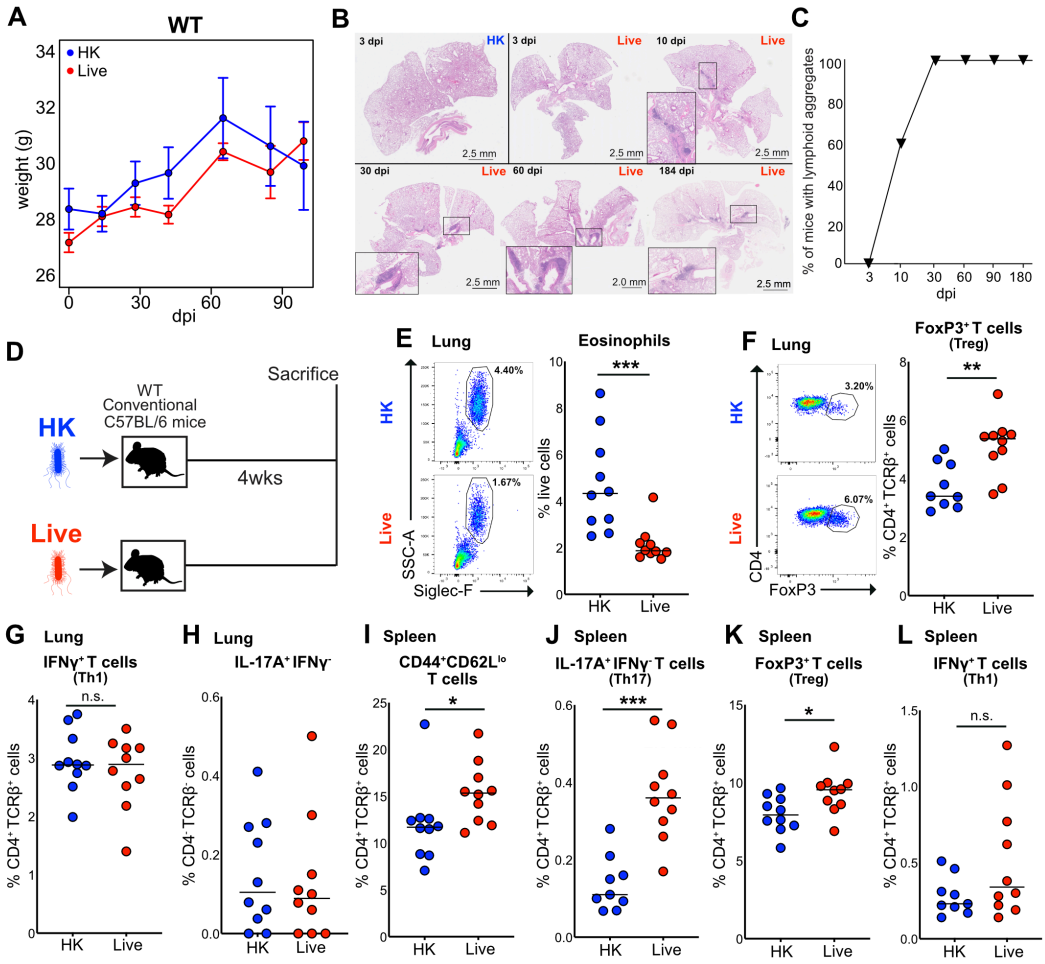

Figure S1 Characterization of *Bordetella pseudohinzii* colonization. Related to Figure 1.

(A) Weight measurements of WT mice inoculated with either HK or live *Bph* for 99 days after initial colonization. Points represent mean +/- SEM. n = 3-10 mice/time point for HK group and n = 4-29 mice/time point.

(B) Representative Hematoxylin and Eosin staining of mice receiving live *Bph* taken 3, 10, 30, 60 and 184 days after inoculation.

(C) Percent of mice demonstrating lymphoid aggregates over a 6-month period (n = 5 mice per time point).

(D) Schematic of the model to investigate the host changes induced by *Bph* colonization. Mice were inoculated with either HK or live *Bph* 4 weeks before tissue collection for immunophenotyping.

(E-L) Flow cytometry of immune cells recovered from lung tissue digests (E-H) or spleens (I-L) from mice 30 days after receiving HK (blue) or live *Bph* (red) inoculation. n = 9-10 mice/group, combined from two independent experiments.

(E) Eosinophils as a percentage of live cells from lung tissue digests. Eosinophils were defined as $Ly6G^-CD11b^+SiglecF^+MHC\text{-}II^-CD11c^-SSC^{hi}$ cells. Representative flow plot on left; quantification on right

(F) Intracellular staining of $FoxP3^+CD4^+$ T cells (Tregs) from the lungs of mice receiving HK or live *Bph*. Percentage expressed as a fraction of $CD4^+TCR\beta^+$ (T-helper) cells.

(G) Intracellular staining of $CD4^+TCR\beta^+IFN\gamma^+$ (Th1) cells from the lungs of mice receiving HK or live *Bph*. Percentage expressed as a fraction of $CD4^+TCR\beta^+$ (T-helper) cells.

(H) Intracellular staining of IL-17A^{+}CD4^{-}TCRβ^{-} cells from the lungs of mice receiving HK or live *Bph*. Percentage expressed as a fraction of CD4^{-}TCRβ^{-} (Non-ab TCR expressing) cells.
(I - L) Percentage of Teff (CD4^{+}TCRβ^{+}FoxP3^{-}CD44^{hi}CD62L^{lo}) cells (I), Th17 cells (CD4^{+}TCRβ^{+}IL-17A^{+}IFNγ^{-}) (J), Treg (CD4^{+}TCRβ^{+}FoxP3^{+}) (K) and Th1 (CD4^{+}TCRβ^{+}IFNγ^{+}) (L) cells from spleen as a percentage of total T-helper cells.

Statistical significance: Wilcox test (A) or Mann-Whitney U test (E-L). Horizontal lines indicate median values. n.s., $p > 0.05$; *, $p < 0.05$; **, $p < 0.01$; ***, $p < 0.001$; ****, $p < 0.0001$.

Figure S2

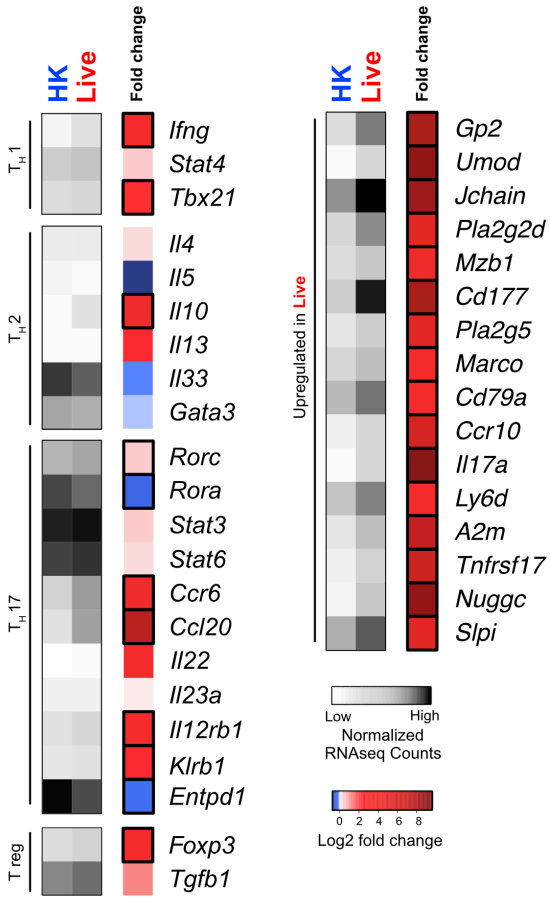

Figure S2 Analysis of immune genes during *Bph* colonization. Related to Figures 2 and 5.
Average normalized read counts for T-helper signature genes and genes consistently upregulated during colonization from HK (left column) and live (middle column) groups are shown in grey. Log2 fold change of each gene is shown on right. Transcripts that were downregulated with colonization are shown in blue while upregulated transcripts are shown in red. Transcripts that are significantly enriched after FDR correction are boxed. Analysis performed in R using DEseq2.

Statistical significance: Wald test with Benjamini-Hochberg correction as implemented in DESeq2.

Figure S3

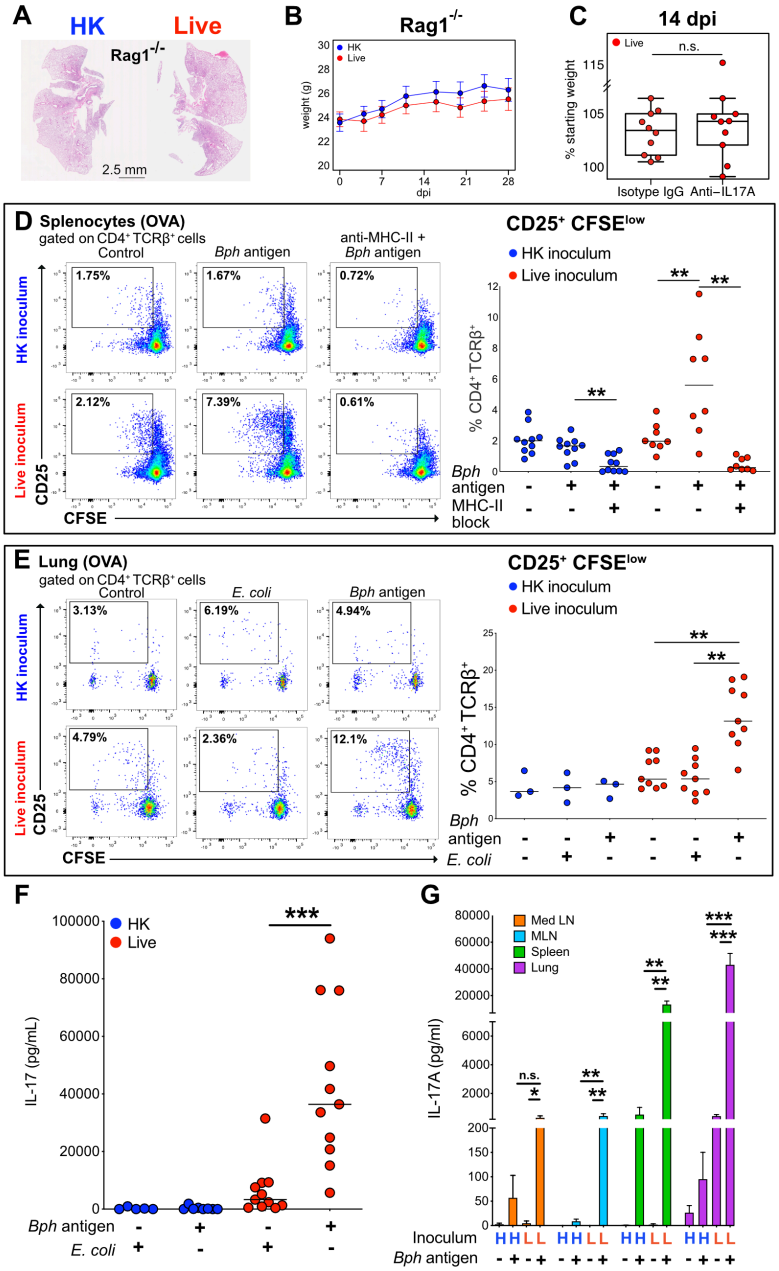

Figure S3 Characterization of antigen-specific T cell response to *Bph*. Related to Figures 3 and 4.

(A) Representative Hematoxylin and Eosin staining of RAG1$^{-/-}$ mice receiving either HK (left panel) or live (right panel) *Bph* taken 30 days after inoculation.

(B) Weight measurements of RAG1$^{-/-}$ mice inoculated with either HK or live *Bph,* n = 4 mice/group. Points represent mean +/- SEM.

(C) Percent starting weight of mice colonized with *Bph* receiving either anti-IL17A monoclonal antibody or isotype control antibody by I.P. injection as shown in Figure 3D. Boxes indicate 25th and 75th percentiles and whiskers are 1.5 x Interquartile range

(D) Left panel: Flow cytometry plots of splenocytes restimulated for 72 h with either no protein (control) or *Bph* proteins from a HK culture. Cells were gated on CD4^{+}TCRβ^{+} cells using CD25 as an activation marker and CFSE as

a proliferation marker. Plots show concatenated data from splenocytes of mice (n = 5 / group) inoculated with either HK or live *Bph* and are representative of two independent experiments. Mice were colonized for 4 weeks before undergoing OVA sensitization and challenge. Right panel: Quantification of $CD25^+$ $CFSE^{lo}$ T cells from splenocyte cultures. n = 9-10 mice / group, combined from 2 independent experiments.
(E) Left panel: Representative flow cytometry plots of restimulated $CD4^+$ T cells lungs of mice after inoculation with either HK or live *Bph* and undergoing OVA sensitization and challenge. Mice were colonized for 7 to 8 weeks before undergoing OVA sensitization and challenge. $CD11c^+$ dendritic cells (DC) were loaded with either no protein, *E. coli* proteins or *Bph* proteins from a HK culture and co-incubated with $CD4^+TCR\square^+$ cells isolated from lung tissue for 72 hours. Cells were gated on $CD4^+TCR\beta^+$ cells using CD25 as an activation marker and CFSE as a proliferation marker. Right panel: quantification of $CD25^+$ $CFSE^{lo}$ lung T-cell and DC co-cultures. n = 3-9 mice / group, combined from 2 independent experiments.
(F) IL-17A ELISA of culture supernatants from lung $CD4^+$ T cells co-cultured with antigen loaded $CD11c^+$ DCs as described in (E). $CD4^+$ T cells were isolated from the lungs of five mice after inoculation with either live or HK *Bph*. n = 4-11 mice / group, combined from 2 independent experiments.
(G) IL-17A ELISA of culture supernatants from T cells co-cultured with DCs as described in (D). $CD4^+$ T cells were isolated from mediastinal lymph node (Med LN), mesenteric lymph node (MLN), spleen or lung of mice 4-8 weeks after inoculation with either HK (H) or live (L) *Bph* before undergoing OVA sensitization and challenge. $CD4^+$ T cells were coincubated with and without *Bph* antigens. Bar plots represent means +/- SEM. n = 6-8 mice / group (HK), n = 11 mice/ group (Live).

Statistical significance: Wilcox test in (B), (C) and (F); or Kruskal-Wallace followed by post-hoc Wilcox test with adjustment of multiple hypotheses using Benjamini-Hochberg correction in (D), (G) and (E). Paired Wilcox test was used for intrasample comparisons; unpaired testing for intersample comparisons. One-tailed testing was used for comparisons between restimulated samples and untreated controls. Horizontal lines indicate median values. n.s., $p > 0.05$; $p > 0.05$; *, $p < 0.05$; **, $p < 0.01$; ***, $p < 0.001$.

Figure S4

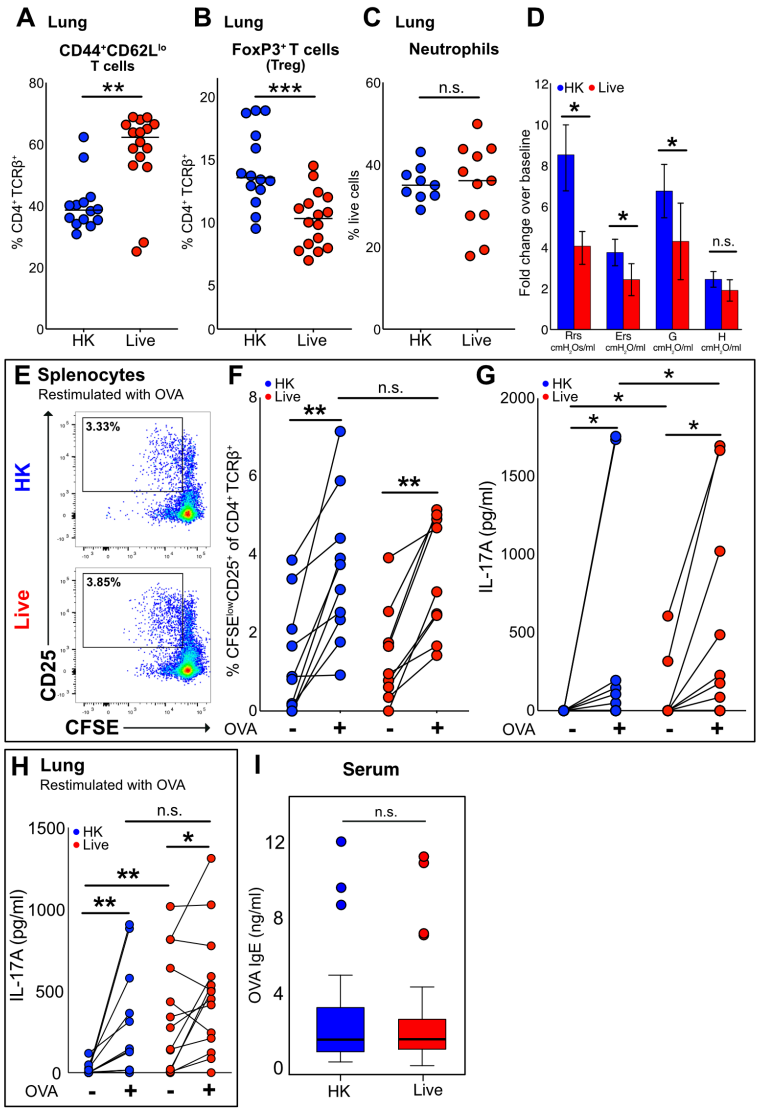

Figure S4 Characterization of the allergic immune response in mice colonized with *Bph*. Related to Figure 3 and 4.

(A-C) Flow cytometry of lung tissue digests from mice 60 days after receiving HK (blue) or live *Bph* (red) inoculation and undergoing OVA sensitization and challenge. n = 9-16 mice/group. Combined from 2-3 independent experiments.

(A) Percentage of Teff ($CD4^+TCR\beta^+FoxP3^-CD44^{hi}CD62L^{lo}$) as a fraction of total T cells.

(B) Intracellular staining for FoxP3 of $CD4^+TCR\beta^+$ cells (T regulatory cells) as a fraction of total T-helper cells.

(C) Neutrophils ($CD11b^+Ly6G^+$) present in tissue, defined as percentage of live cells.

(D) Change in respiratory resistance (Rrs) respiratory elastance (Ers), tissue dampening (G), tissue elastance (H) in mice undergoing challenge with 25 mg/ml methacholine. Data are normalized for each mouse to airway measurements before undergoing methacholine challenge. Experiments were performed using a Flexivent FX1. Bars represent mean +/- SEM. n = 8 mice/group.

(E - G) Assessment of OVA specific responses in mice inoculated with either live or HK *Bph* and undergoing AAI.

(E) Concatenated flow cytometry plots of splenocytes from mice receiving either HK or live *Bph* then restimulated with OVA. Mice were colonized for 4 weeks before undergoing OVA sensitization and challenge. Splenocytes were loaded with either no protein or OVA for 72 h. Flow plots show concatenated data from 5 mice and are representative of two independent experiments.
(F) Quantification of $CD25^{+}CFSE^{lo}$ T cells from splenocyte cultures. n = 9-10 mice / group, combined from 2 independent experiments.
(G) IL-17A ELISA of culture supernatants from splenocyte cultures as described in (E). n = 15-17 mice / group, combined from 3 independent experiments.
(H) IL-17A ELISA of culture supernatants from lung T cells co-cultured with DCs loaded with either no protein or OVA for 72 h as described in (E). Mice were colonized from 4 to 8 weeks before undergoing OVA sensitization and challenge. n = 8-11 mice / group, combined from 3 independent experiments.
(I) ELISA to quantify ovalbumin specific IgE from the sera of mice undergoing OVA sensitization and challenge. Box indicates 25th and 75th percentiles and whiskers are 1.5 x Interquartile range. n = 48 and 55 mice for HK and live groups, respectively, combined from 8 independent experiments.

Statistical significance: Mann-Whitney U test in (A - C) and (I); Wilcox test in (D); or Kruskal-Wallace followed by post-hoc Wilcox test with adjustment of multiple hypotheses using Benjamini-Hochberg correction in (F), (G) and (H). Paired, one-way Wilcox test was used for intrasample comparisons; unpaired, two-way Wilcox test was used for intersample comparisons. Horizontal lines indicate median values. n.s., $p > 0.\ 05$; *, $p < 0.05$; **, $p < 0.01$; ***, $p < 0.001$.

Figure S5

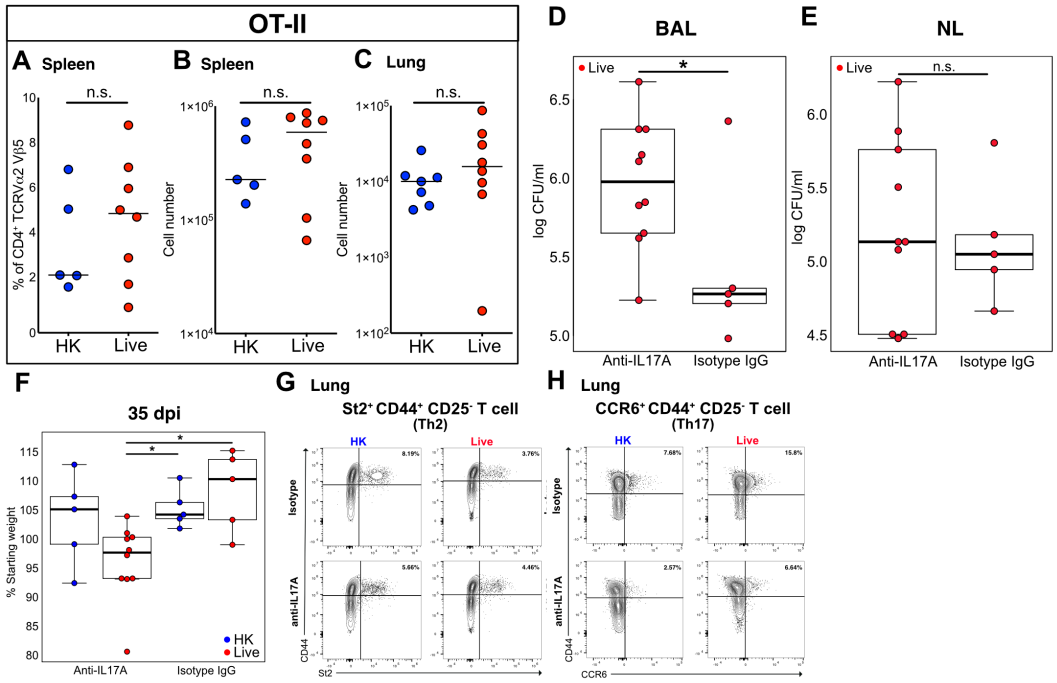

Figure S5 Characterization of T cell responses in mice colonized with *Bph* while experiencing allergic airway inflammation. Related to Figure 4.

(A-C) Percentage and number of OVA-specific T cells (OTII) recruited to the lung and spleen of mice either inoculated with HK or live *Bph* 20 days before receiving 50,000 OTII T cells then undergoing OVA sensitization and challenge. n = 7-8 mice/group, combined from 2 independent experiments.

(A) Percentage of CD4+ T cells ($CD4^+CD45.1^+$) expressing the OT-II receptor ($V\alpha2^+V\beta5^+$) recruited to the spleen.

(B) Numbers of OT-II $CD4^+$ T ($CD4^+CD45.1^+V\alpha2^+V\beta5^+$) cells recruited to the spleen.

(C) Numbers of OT-II $CD4^+$ T ($CD4^+CD45.1^+V\alpha2^+V\beta5^+$) cells recruited to the lung.

(D) CFU of Bph recovered from BALs of mice treated with either anti-IL-17A or isotype control antibody collected at the time of sacrifice (35 dpi). n = 5-10 mice / group.

(E) CFU of Bph recovered from nasal lavages of mice treated with either anti-IL-17A or isotype control antibody collected at the time of sacrifice (35 dpi). n = 5-10 mice / group.

(F) Weight as a percentage of starting weight at the time of sacrifice (35 dpi) for HK (blue) of Live (red) *Bph* inoculum groups. Mice were treated with either anti-IL-17A antibody or isotype control and underwent OVA sensitization and challenge. n = 5-10 mice / group.

(G) Representative flow plots of T cells ($CD45^+CD4^+TCR\beta^+CD25^-$) gated on $CD44^+St2^+$ for Th2 cells. Columns are HK (left) of Live (right) *Bph* inoculum groups. Rows are isotype (top) or anti-IL-17A treated (bottom).

(H) Representative flow plots of T cells ($CD45^+CD4^+TCR\beta^+CD25^-$) gated on $CD44^+CCR6^+$ for Th17 cells. Columns are HK (left) of Live (right) *Bph* inoculum groups. Rows are isotype (top) or anti-IL-17A treated (bottom).

Statistical significance: Mann-Whitney U test in (A - C); One-tailed Wilcox test in (D - E); or Kruskal-Wallace followed by post-hoc Wilcox test with adjustment of multiple hypotheses using Benjamini-Hochberg correction in (F). Horizontal lines indicate median values. Box indicates 25th and 75th percentiles and whiskers are 1.5 x Interquartile range. n.s., $p > 0.05$; *, $p < 0.05$.

Figure S6

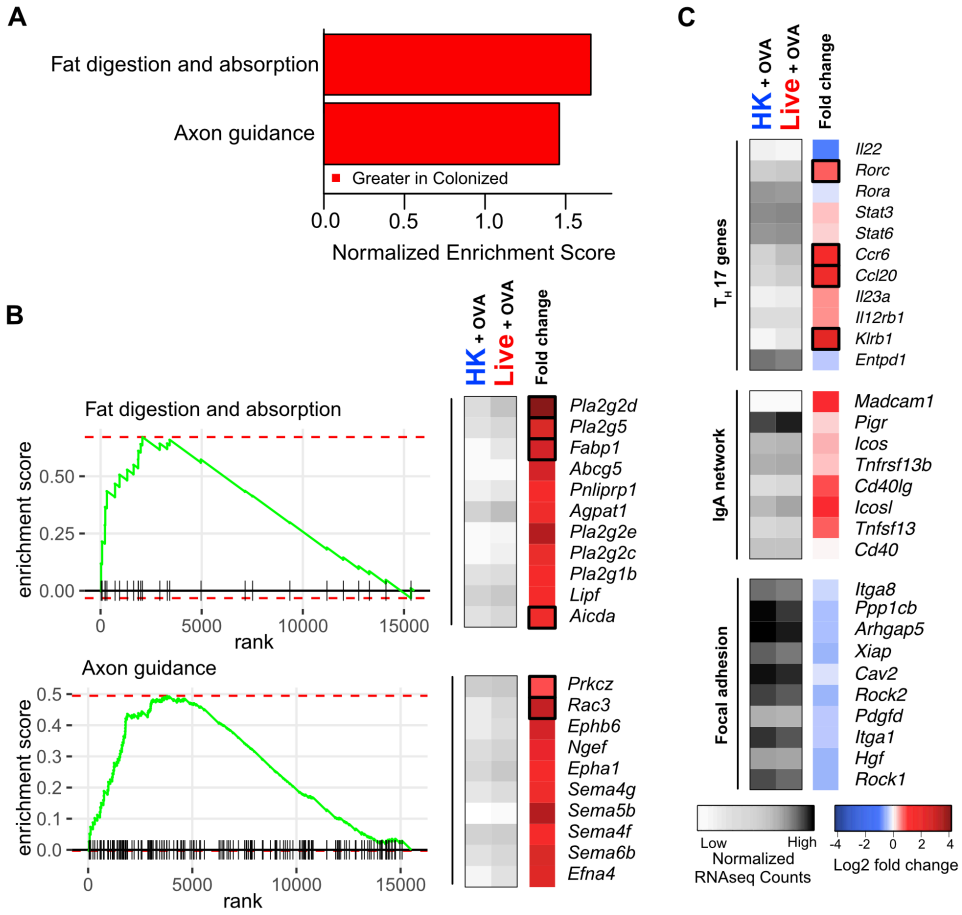

Figure S6 Additional analysis of Lung Transcriptomic Data from Mice Colonized with *Bph* undergoing OVA Sensitization and Challenge. Related to Figures 2 and 5.

(A) KEGG pathways enriched in mice receiving a live compared to HK *Bph* inoculum. Only pathways with an adjusted p value < 0.05 are shown with their normalized enrichment score. n = 5 / group

(B) Enrichment plots and heatmaps of selected pathways. On left, enrichment plots for KEGG pathways are shown and on the right of each panel, a heatmap demonstrating normalized read counts and fold change of select leading-edge genes from each KEGG pathway. Average normalized read counts for HK (left column) and Live (middle column) groups are shown in grey, while log2 fold change of each gene is shown in the rightmost column in blue, white and red. Genes that are significantly enriched after FDR correction are boxed. Analysis performed in R using DEseq2.

(C) Heatmap of genes from KEGG pathways identified in Figure 2 that were no longer enriched after OVA sensitization and challenge.

Statistical significance: GSEA statistic as implemented in fgsea (Sergushichev, 2016) (A) or the Wald test with Benjamini-Hochberg correction as implemented in DESeq2 in (B - C).

Figure S7

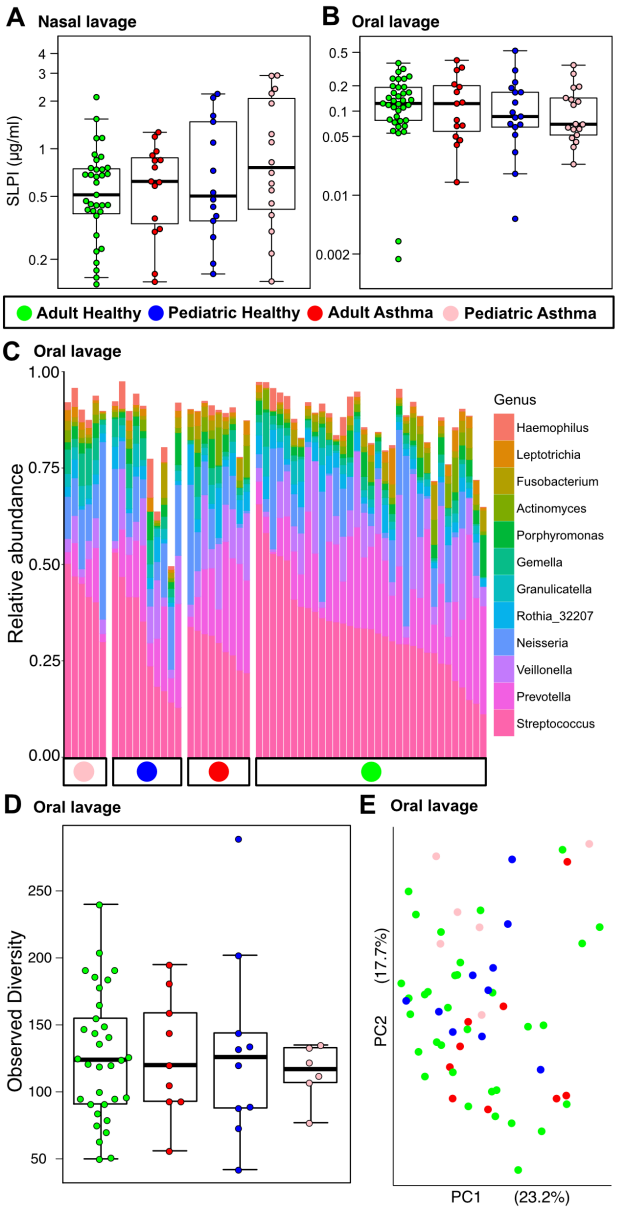

Figure S7 SLPI abundance and Microbial Ecology Upper Airway Specimens of Healthy and Asthmatics. Related to Figure 6.

(A) SLPI concentrations from nasal lavage specimens from MARS study participants divided by age and disease cohorts.

(B) SLPI concentrations from oral lavage specimens from MARS study participants divided by age and disease cohorts.

(C) Genus-level taxonomic overview of oral microbial communities from each study group. Taxonomy was determined from V4-16S rRNA as described in Methods. Each vertical bar represents a single study participant.

(D) Observed species for each study group.

(E) Principal Coordinates analysis of Bray-Curtis distances between oral lavage specimens.

Statistical significance: Kruskal-Wallace test in (A), (B) and (D). Box indicates 25th and 75th percentiles and whiskers are 1.5 x Interquartile range.